Thermodynamic correlation of molecular simulation data

Rolf Lustig
Department of Chemical and Biomedical Engineering, Cleveland State University, Cleveland, Ohio 44115, USA

Gabor Rutkai and Jadran Vrabec
Lehrstuhl für Thermodynamik und Energietechnik, Universität Paderborn, 33098 Paderborn, Germany

Corresponding author: Rolf Lustig, Department of Chemical and Biomedical Engineering, Cleveland State University, Cleveland, Ohio 44115, USA, Email: r.lustig@csuohio.edu

Abstract

Strategies to fit molecular simulation data sets to low parameter fundamental equation of state correlations are reported. The Lennard-Jones model system truncated and shifted at interatomic distance $r_c/\sigma = 2.5$ is used as an example. Homogeneous fluid states, vapor-liquid equilibrium including estimation of the critical point, and the Joule-Thomson inversion curve are investigated. The results suggest that small molecular simulation data sets at homogeneous states are sufficient to provide consistent thermodynamic information over large portions of the fluid state.

Keywords: thermodynamic correlation, molecular simulation, equation of state

1 Introduction

Molecular simulation has evolved to a point of general acceptance in the applied sciences. It is therefore natural to promote its potential use in engineering. Due to low cost computational hardware capabilities, thermodynamic property files of arbitrary size can be generated on a time scale of days. Such unlimited data files, however, are of little value for practical engineering. For practical benefit, molecular simulation data must be rationalized by correlation to serve as inter- and extrapolation schemes. Data correlations are typically done for special purposes, such as phase equilibrium data, or thermal equations of state (EOS) relating pressure p, density ρ, temperature T ($p\rho T$) data. Complete thermodynamic knowledge, including the above, is given by thermodynamic fundamental equation of state (FEOS) correlation. Although EOS and FEOS correlation for molecular simulation data exist [1, 2, 3, 4, 5, 6, 7, 8, 9, 10, 11, 12, 13, 14, 15, 16], they constitute a negligible fraction of the molecular simulation literature. Molecular simulators tend to publish selective data, such as phase equilibrium data, which are interesting and needed, but not ready for use in process designs. In this work we are not interested in matching molecular models to real compounds. The effort is on the investigation of thermodynamic correlation possibilities for model systems only, in particular FEOS correlation.

The use of model systems in molecular simulation is a statistical mechanical exercise. It is therefore natural to attempt correlation of molecular simulation data with as much theoretical evidence as possible [5]. Thermodynamic perturbation theory is one very successful underlying strategy for such an approach [17, 18]. The two currently best FEOS correlations for the Lennard-Jones system [5, 6] are prime examples for the power of the hard body reference system approach in FEOS correlations. The underlying statistical mechanical hard body theory for molecular fluids is due to Boublik, Nezbeda, and their coworkers as summarized in reference [19]. The resulting semi-empirical FEOS correlations [5, 6] are by far superior to earlier fully empirical correlations [2, 4].

The perturbation theoretical approach to thermodynamic correlation, however, may require specifics beyond simple for more complex molecular models. In such cases semi-empirical approaches may very well become impracticable. Fully empirical correlations may still be tried. They divide into two classes: Compound specific correlations and compound group specific correlations. The former class of correlations is intended to rationalize thermodynamic data as accurate as possible, which requires sophisticated numerical optimization strategies, individually applied to each compound under consideration. References [20, 15, 16] are recent examples. The latter class of correlations is intended to cover groups of fluids.

An example is the group of non-polar fluids as opposed to the group of polar fluids. The former class of correlations requires a very high degree of expertise due to simultaneous correlation and optimization of mathematical models. The latter class of correlations reduces to pure fitting given a mathematical model, which is straightforward and may be automated. In this work we focus on identifying all-purpose correlations which may be added to any molecular simulation package for rationalizing vast amounts of thermodynamic data for any group of fluids. Some guidelines are established to maximize profits of fully empirical thermodynamic correlation.

To date, successful FEOS correlation development exclusively stems from the employment of real laboratory data for real compounds [21, 22]. In the present work we investigate to what extent state-of-the-art knowledge can be transfered to model systems as they are used in molecular simulation. Span [22] assessed the quality of FEOS correlations as follows.

(1) Group one reference FEOS: Scientific standard for equipment calibration and evaluation. FEOS for about 10 compounds fall in this class. Examples are argon, nitrogen, carbon dioxide, water, methane, and ethylene. The number of fit parameters is around 50.

(2) Group two reference FEOS: Aim at reaching the standards of group one reference FEOS, but are prohibited by less accurate experimental data. Available for some 20 technically important substances, such as rare gases, lower alkanes, alcohols, refrigeration fluids, and air. The number of fit parameters is around 30.

(3) Group three or technical FEOS: These FEOS aim at a significantly improved performance over cubic type EOS, as they are discussed in reference [23]. Alternatives, considered here are based on fully empirical low parameter modified Benedict-Webb-Rubin (MBWR) [24] type FEOS, as advocated by Span [22]. To date, about 100 compounds have been treated by such an approach. The number of fit parameters is around 15.

Molecular simulation, as an alternative source of thermodynamic data generation, can not replace real laboratory experiments in general. However, it is believed to constitute a credible complement [25, 26, 27]. In particular, thermodynamic properties not directly measurable in the laboratory, are rigorously accessible in molecular simulation. A recent study on a variety of distinct compounds has uniquely verified such claims [20]. Group one reference FEOS can presently not be the target of molecular simulation. However, the lower end of group two reference FEOS and the full range of group three FEOS may. Therefore, the present work is an attempt to investigate technical grade FEOS correlations using molecular simulation data. These low parameter FEOS correlations were simultaneously optimized for a variety of real fluids. They are therefore candidates for routine correlations of thermodynamic data from molecular simulation as discussed above. With this work we begin planned investigations of the usefulness of laboratory-based correlation strategies, using the Lennard-Jones truncated and shifted (LJTS) model fluid as a first example.

The paper is organized as follows. Section 2 describes low parameter FEOS correlations. The model fluid is specified in section 3. Section 4 details the generated data set and subsequent manipulations. Some details of fitting procedures are outlined in section 5. Section 6 presents results. Conclusions are drawn in section 7.

2 Low parameter FEOS correlations

State-of-the-art FEOS correlations stem from utilization of experiments for real compounds. Thermodynamic properties directly accessible in the laboratory are restricted to $p\rho T$ data, heat capacities, and speeds of sound. Occational use of phase equilibrium data or virial coefficients does not extend the available data, since they are still $p\rho T$ data. As mentioned in section 1, this work focusses on group three or technical grade FEOS correlations. Span's requirements for technical accuracy are [22, sec. 6.2]:

(1) In homogeneous states, density must be reproduced within $\pm 0.2\%$ for $p < 300$ bar and $\pm 0.5\%$ for $p < 1000$ bar.

(2) In homogeneous states, heat capacity and/or speed of sound must be reproduced within $\pm 2\%$.

(3) Vapor-liquid equilibrium must be reproduced within 0.2% for vapor pressure and bubble density, and within 0.4% for dew density. The immediate vicinity of the critical point is excluded.

Technically and scientifically most important fluid states [22, sec. 5] are temperatures up to $T = 500$ K and pressures up to $p = 300$ bar. In molecular simulation, model systems replace real compounds. As explained in section 3, temperature and pressure in physical units have no immediate counterpart in molecular simulation. Global statements on accuracy requirements for thermodynamic properties then require reference states, which exist for both real compounds and molecular models, such as the critical point or others. Here, we suggest a rule of thumb stating that 300 bar corresponds to roughly five times the critical pressure p_c for a large amount of technically relevant compounds. Assement of an upper limit of temperature requires ambiguity. However, other rules of thumb exist for both real compounds and molecular models relating characteristic temperatures. For methane, 1000 K corresponds to roughly five times the critical temperature T_c. In section 6.3 we indicate how such ratios may be approximated for molecular models by statistical mechanics. The first of the above accuracy requirements for group three FEOS correlations using molecular simulation data is then (quite arbitrarily) redefined:

(1) The most important fluid states are limited by $T/T_c < 2.5$. The highest technically relevant temperature is considered to be $T/T_c = 5$. In homogeneous states, density must be reproduced within $\pm 0.2\%$ for $p/p_c < 5$ and $\pm 0.5\%$ for $p/p_c < 20$.

The above suggests that $T/T_c < 2.5$, $p/p_c < 5$ are primary and $T/T_c < 5$, $p/p_c < 20$ are secondary state point margins for data sets to be used in routine correlation of molecular simulation data to technical grade FEOS correlations.

In correlation work one typically uses dimensionless independent variables such as

$$\tau \equiv T_r/T\,, \quad \text{and} \quad \delta \equiv \rho/\rho_r\,, \tag{1}$$

where T_r and ρ_r are reference values, which may or may not be the critical values T_c or ρ_c. If they are the critical values, then $\tau_c = \delta_c = 1$, as supported by the theorem of corresponding states, which becomes vital in sections 5 and 6.

It is common to decompose the Helmholtz energy $A(\tau,\delta)$ into a residual part $A^r(\tau,\delta)$ and a part relating to an ideal gas $A^i(\tau,\delta)$ at the same temperature and density by [28]

$$\frac{A(\tau,\delta)}{Nk_BT} \equiv \frac{a(\tau,\delta)}{k_BT} \equiv \alpha^r(\tau,\delta) + \alpha^i(\tau,\delta)\,, \quad \text{or} \quad \frac{\partial^{m+n}\alpha(\tau,\delta)}{\partial\tau^m\partial\delta^n} \equiv \alpha_{mn}(\tau,\delta) = \alpha^r_{mn}(\tau,\delta) + \alpha^i_{mn}(\tau,\delta)\,. \tag{2}$$

One is left with a correlation of the residual part of the total Helmholtz energy. The ideal part can be obtained by independent means. Eq. (6) in section 3 is a simple example. We identified four low parameter FEOS correlations for the present paper: One 10 parameter FEOS [22, sec. 7], two 12 parameter FEOS [22, 29, 30], and one 14 parameter FEOS [31]. The structure of these four FEOS correlations are identical and of MBWR type

$$\frac{A^r(\tau,\delta)}{Nk_BT} \equiv \frac{a^r(\tau,\delta)}{k_BT} \equiv \alpha^r(\tau,\delta) = \sum_{i=1}^{I} n_i f_i(\tau,\delta) = \sum_{i=1}^{I_P} n_i\tau^{t_i}\delta^{d_i} + \sum_{i=I_P+1}^{I_P+I_E} n_i\tau^{t_i}\delta^{d_i}\exp(-\gamma_i\delta^{p_i})\,, \tag{3}$$

with $I = 10, 12, 14$ basis functions $f_i(\tau,\delta)$: I_P polynomials and I_E combinations of polynomials and density dependent exponentials. The most important and most difficult part of FEOS correlation is the simultaneous establishment of optimized sets I_P, I_E, and the particular exponents t_i, d_i, p_i, and γ_i. Traditional trial and error optimization strategies for the purpose are nowadays replaced by sophisticated procedures based on genetic algorithms [22], methods borrowed from statistical mechanics, such as simulated annealing [32, 31], or non-linear deterministic schemes [33]. In all previous work on generalized correlations [22, 29, 30, 31], $\gamma_i = 1$. This paper is not the place to ponder optimization procedures, however, since we use the outcomes, some observations must be communicated.

Table 1 shows details of the selected FEOS correlations. The Span-Wagner 12 parameter FEOS were designed separately for non-polar (SW_{12}) and polar (SW^p_{12}) compounds, because both types of compounds could not be satisfactorily fitted with identical 12 basis functions [22, 29, 30]. We assume that

the notion polar refers to the presence of permanent multipole moments such as dipoles or quadrupoles. The Sun-Ely 14 parameter FEOS (SE_{14}) is an attempt to cover both non-polar and polar compounds in one single correlation [31]. Obviously, the number of basis functions needed an increase from 12 to 14. We explain in Table 1 why we consider the SE_{14} FEOS a minor alteration of the original developments of Span and Wagner.

Molecular simulation, as a numerical experiment, comes with errors, including fundamental statistical uncertainties, systematic errors, and possible correlations among the two. We treat statistical errors in molecular simulation data sets thoroughly [34, 35, 36], but we ignore possible systematic errors. In this paper we are devoted to the concept of stability of empirical FEOS, which has been discussed by Span [22]. Stability of FEOS correlation assesses both transferability from one compound to another and insensitivity to the size of underlying data sets, all with identical basis functions. Span shows that reducing the number of basis functions from 12 to 10 (S_{10}, by two only) not only increases the stability of a FEOS correlation, it increases it significantly [22]. He also shows that thinning a large data set from thousands of data to some ten may not have a significant effect on accuracy of such FEOS correlations. Here, we investigate such findings for routine correlation of molecular simulation data.

3 A simple realistic model fluid

The LJTS model system used here is a prototype of a perfectly simple realistic non-polar model fluid, defined by a pair potential $u = u(r)$ according to

$$u_{\mathrm{LJTS}}(r) = \begin{cases} u_{\mathrm{LJ}}(r) - u_{\mathrm{LJ}}(r = 2.5\sigma)\,, & \text{for} \quad r \le 2.5\sigma \\ 0\,, & \text{for} \quad r > 2.5\sigma \end{cases} \quad , \quad \text{with} \quad u_{\mathrm{LJ}}(r) = 4\varepsilon \left[\left(\frac{\sigma}{r}\right)^{12} - \left(\frac{\sigma}{r}\right)^{6} \right] . \tag{4}$$

The potential parameters ε and σ denote the minimum energy and the distance r where the energy goes through zero. They provide a molecular energy and length scale which can be used to reduce any thermodynamic property to dimensionless numbers of order unity. Examples are

$$T^* = k_{\mathrm{B}}T/\varepsilon\,, \quad \rho^* = \rho\sigma^3\,, \quad p^* = p\sigma^3/\varepsilon\,, \quad e^* = e/\varepsilon\,, \quad s^* = s/k_{\mathrm{B}}\,, \quad c_v^* = c_v/k_{\mathrm{B}}\,, \quad \ldots \tag{5}$$

for temperature T, density ρ, pressure p, internal energy e, entropy s, isochoric heat capacity c_v, and so on. The scheme is similar to eq. (1) by using $T_{\mathrm{r}} = \varepsilon/k_{\mathrm{B}}$ and $\rho_{\mathrm{r}} = \sigma^{-3}$. It is common practice to use stars as superscripts for reduced quantities, which is unfavorable here, due to multiple superscripts and subscripts in FEOS correlations. Therefore, we omit stars with the understanding that reduced quantities are indeed referred to. Note that τ and δ in eq. (1) are unchanged in the starred system of units. Furthermore, we use lower case letters for molar quantities (per particle, for example $s = S/N$).

The LJTS system is a classical (c) atomic interaction model for which the ideal part of the Helmholtz energy in eq. (2) is $\alpha^{\mathrm{i}}_{mn} = \alpha^{\mathrm{i,c}}_{mn}$ with [37]

$$\left[\alpha^{\mathrm{i,c}}_{mn}(\tau,\delta)\right] = \begin{bmatrix} \frac{3}{2}\ln\tau + \ln\delta & \delta^{-1} & -\delta^{-2} & \cdots \\ \frac{3}{2}\tau^{-1} & 0 & 0 & \cdots \\ -\frac{3}{2}\tau^{-2} & 0 & 0 & \cdots \\ \vdots & \vdots & \vdots & \ddots \end{bmatrix} , \quad \text{for} \quad m, n \ge 0\,. \tag{6}$$

We have very recently proposed a fully optimized FEOS correlation for the LJTS model fluid [15]

$$\alpha^{\mathrm{r}}(\tau,\delta) = \sum_{i=1}^{6} n_i \tau^{t_i} \delta^{d_i} + \sum_{i=7}^{12} n_i \tau^{t_i} \delta^{d_i} \exp(-\delta^{p_i}) + \sum_{i=13}^{21} n_i \tau^{t_i} \delta^{d_i} \exp\left[-\chi_i(\tau - \epsilon_i)^2 - \eta_i(\delta - \varphi_i)^2\right] . \tag{7}$$

The model is of type eq. (3) augmented by nine Gaussians with additional parameters χ_i, ϵ_i, η_i, φ_i for enhanced accuracy. With 21 terms this compound specific correlation essentially represents all known molecular simulation data (Section 4) within their estimated uncertainty. In this work we use eq. (7) as a benchmark for generalized correlations of type eq. (3).

4 Data set

The data set used in this work is identical to the one used for the development of the benchmark FEOS correlation [15]. Our open source molecular simulation tool *ms*2 [36] was used to generate a variety of thermophysical properties at 705 state points in NVT molecular dynamics mode. Thermodynamic data include pressure p, residual internal energy e^{r}, volume derivative of the residual internal energy $(\partial e^{\mathrm{r}}/\partial v)_T$, and residual isochoric heat capacity c_v^{r}. 1372 LJTS particles were sufficiently equilibrated and then run for 2 to 5 million production time steps of length $t^* = t/(\sigma\sqrt{m/\varepsilon}) = 0.001$.

System size effects were investigated and found to be irrelevant for the purpose of this work [15]. Note that the LJTS model is designed to not involve any bias through potential energy cut-offs.

Figure 1 (top left) shows the original data set in the T, ρ plane. The highest temperature is $T = 11 \approx 10T_{\mathrm{c}}$ (about 2000 K for methane). The highest pressure is $p = 6.8 \approx 70p_{\mathrm{c}}$ (about 3000 bar for methane). Those limits hugely exceed the projected range of accurate data correlation as indicated in section 2. State points were selected to not be within neither the vapor-liquid nor the liquid-solid two-phase region. The former condition is secured because the vapor-liquid phase equilibrium of the LJTS system is known [38]. The liquid-solid phase equilibrium is unknown, therefore the molecular simulation strategy advocated here suffers from ignorance of possible solid states in the original data set. We did encounter this problem with a significantly larger original data set. Deviation plots as in section 6.1 revealed gross outliers at high density. In all cases the diffusion coefficient (which is measured in our tool) dropped by orders of magnitude. Such state points must then be removed from the data set. In summary, an oversized data set is available, allowing for investigations of varying fitting conditions as indicated in Figure 1. Generalized FEOS correlations and their verifications can be tested against the raw data and the benchmark FEOS based on the same data set.

5 Fits

According to eqs. (2), (3), (6), and the outlines in reference [39], multiproperty fits require data (with parameters T_{r} and ρ_{r}) for $\alpha^{\mathrm{r}}_{mn}(\tau, \delta)$. The properties measured in the current application of *ms*2 yield

$$\alpha^{\mathrm{r}}_{01} = \left(\frac{p}{\rho T} - 1\right)\delta^{-1}\,, \quad \alpha^{\mathrm{r}}_{10} = e^{\mathrm{r}}\,T_{\mathrm{r}}^{-1}\,, \quad \alpha^{\mathrm{r}}_{11} = -\left(\frac{\partial e^{\mathrm{r}}}{\partial v}\right)_T \delta^{-2}\,T_{\mathrm{r}}^{-1}\rho_{\mathrm{r}}^{-1}\,, \quad \alpha^{\mathrm{r}}_{20} = -c_v^{\mathrm{r}}\,\tau^{-2}\,. \tag{8a}$$

Since we intend weighted fits, we apply the standard error propagation law with the statistical errors Δ_p, $\Delta_{e^{\mathrm{r}}}$, $\Delta_{(\partial e^{\mathrm{r}}/\partial v)_T}$, and $\Delta_{c_v^{\mathrm{r}}}$ to eqs. (8a) to yield approximately

$$\Delta_{\alpha^{\mathrm{r}}_{01}} = \frac{\Delta_p}{\rho T}\,\delta^{-1}\,, \quad \Delta_{\alpha^{\mathrm{r}}_{10}} = \Delta_{e^{\mathrm{r}}}\,T_{\mathrm{r}}^{-1}\,, \quad \Delta_{\alpha^{\mathrm{r}}_{11}} = \Delta_{(\partial e^{\mathrm{r}}/\partial v)_T}\,\delta^{-2}\,T_{\mathrm{r}}^{-1}\rho_{\mathrm{r}}^{-1}\,, \quad \Delta_{\alpha^{\mathrm{r}}_{20}} = \Delta_{c_v^{\mathrm{r}}}\,\tau^{-2}\,. \tag{8b}$$

If the critical point of a fluid is known precisely, it would typically serve as a constraint in FEOS correlation. In that case, $T_{\mathrm{r}} = T_{\mathrm{c}}$ and $\rho_{\mathrm{r}} = \rho_{\mathrm{c}}$ are enforced to yield $\tau_{\mathrm{c}} = \delta_{\mathrm{c}} = 1$, which is vital for corresponding states considerations [40]. If the critical point is unknown, a guess for T_{r} and ρ_{r} is necessary. An *a posteriori* computation of the critical point will most likely yield $T_{\mathrm{r}} \neq T_{\mathrm{c}}$ or $\rho_{\mathrm{r}} \neq \rho_{\mathrm{c}}$ or both. In this situation the computed critical point becomes a function of the assumed reducing parameters. Although the vapor-liquid phase equilibrium including the critical point of the LJTS system are known approximately [38, 15], we do not use this knowledge for the fits, as discussed in more detail in section 7. Here we emulate the most likely scenario that the critical point of a model fluid is not known. We investigate to what extent generalized FEOS correlation of only homogeneous state data can find a natural unconstrained critical point which occurs at $\tau_{\mathrm{c}} = \delta_{\mathrm{c}} = 1$:

(1) Use T_{r} and ρ_{r} to form $\tau = T_{\mathrm{r}}/T$ and $\delta = \rho/\rho_{\mathrm{r}}$ in eq. (1).

(2) Perform the FEOS fit with molecular simulation data, weighted by their uncertainties.

(3) Use the FEOS correlation to determine a critical point $T_{\mathrm{c}}, \rho_{\mathrm{c}}$. If the reducing (r) and critical (c) points do not agree to satisfaction, update $T_{\mathrm{r}} \equiv T_{\mathrm{c}}$, $\rho_{\mathrm{r}} \equiv \rho_{\mathrm{c}}$, and go back to (1).

In essence, the current implementation operates as follows. Given initial reducing parameters, which need not be precise, a preliminary FEOS is fitted. Then, isothermal vapor-liquid equilibrium is determined starting at low temperature using equality of chemical potentials versus pressure in both phases. Full use is made of the preliminary FEOS correlation in some Newton-Raphson scheme. With increasing temperature, the procedure will cease to yield "phase equilibrium" with distinct coexisting densities: The critical temperature has been surpassed and two limiting temperatures are at disposal for refinement. Extrapolation of the rectilinear diameter [40] to the critical temperature determines a critical density ρ_c to be used for ρ_r in the next pass. Upon convergence, the critical point conditions $(\partial p/\partial\rho)_{T=T_c} = (\partial^2 p/\partial\rho^2)_{T=T_c} = 0$ are automatically fulfilled. If the underlying data set is within the projected limits in section 2, the procedure iterates to arbitrary numerical accuracy.

Except for our very recent own work [20, 15], to the best of our knowledge, EOS or FEOS correlation from molecular simulation has never been performed with data other than $p\rho T$ data and residual internal energies e^r. Examples for such standards are the currently best semi-empirical FEOS for the full Lennard-Jones system by Kolafa and Nezbeda [5] and Mecke *et al.* [6]. Occasional uses of virial coefficients do not extend the physical data pool: Virial coefficients are still sole $p\rho T$ data. Here, we limit our investigations to:

(1) Use current standards ($p\rho T$, e^r) to assess the generalized FEOS correlations in section 2. Investigate stability by reducing the data set.

(2) Increase the number of thermodynamic properties used in the fits.

Fitting procedures employed in this work follow the outlines of Hust and McCarthy [39] for weighted multiproperty fits with or without constraints. Quantities needed are: Identification of properties $p = 1 \cdots P$, state points $m = 1 \cdots M(p)$, thermodynamic properties x_{pm} from molecular simulation with their associated uncertainties $\Delta_{x_{pm}}$, and the corresponding properties x_{pm}^{FEOS} resulting from the correlation. As mentioned in section 2, associated uncertainties $\Delta_{x_{pm}}$ are purely statistical and were obtained as described in references [34, 35, 36]. Quality assessments of FEOS correlations are then attempted by what may be called the overall weighted deviation

$$\sigma_{PM} = \left[\frac{\sum_{p=1}^{P} \sum_{m=1}^{M(p)} \left(\Delta x_{pm}\right)^2 / \Delta_{x_{pm}}^2}{\sum_{p=1}^{P} M(p) - I} \right]^{1/2}, \quad \text{with} \quad \Delta x_{pm} \equiv x_{pm} - x_{pm}^{\mathrm{FEOS}}, \tag{9}$$

where I is the number of correlation parameters in eq. (3). The denominator represents the degree of freedom of the fit problem. In general, the smaller σ_{PM}, the closer the fit data are to the underlying experimental data. More detailed, the following fit scenarios are possible:

1) $\sigma_{PM} \approx 1$: The correlation properly represents the underlying data set essentially within all uncertainties.

2) $\sigma_{PM} >> 1$: The number of correlation parameters is insufficient, uncertainties $\Delta_{x_{pm}}$ are underestimated i.e. reported too low, or both.

3) $\sigma_{PM} << 1$: Data noise is fitted, the number of correlation parameters is too high.

All reported x in this work relate to p, e^r, $(\partial e^r/\partial v)_T$, c_v^r.

6 Results

Span [22, sec. 7.2.2.3] describes a dramatic reduction of a data set for methane from more than thousand data to about 10, without significant detoriation of the FEOS correlation (S_{10}), thereby proving extraordinary stability. It is therefore natural to investigate effects of such reduction for data sets from molecular simulation. For the purpose, we discriminate data reduction into shrinking and thinning. Shrinking is reducing the margins of state points, keeping data within. Thinning is removing state points from a data set within given margins. Span's reduction of the data set for methane is thinning.

Table 2 quantifies both kinds of reductions illustrated in Figure 1. As indicated in section 2, low parameter FEOS correlations with technical accuracy were optimized with data sets not exceeding the margins $T/T_c < 2.5$ and $p/p_c < 5$, which corresponds to the data set $M = 271$ in Figure 1 and Table 2. The technically relevant margins $T/T_c < 5$ and $p/p_c < 20$ with $M = 481$ state points are considered upper limits for sensible applications. In this section we report some very general findinds for the FEOS correlations considered. The quantities used for the fits are $\alpha^r_{01}, \alpha^r_{10}$ from p, e^r. More detailed analyses follow in subsequent sections.

As discussed in section 5, it is possible to find reducing parameters T_r and ρ_r so that $\tau_c = \delta_c = 1$ simultaneously. Table 2 shows that the SW^p_{12} and SE_{14} FEOS with the oversized data set $M = 705$ are the only exceptions. In those two cases we were unable to enforce convergence of the overall iteration procedure described in section 5. If one of the conditions $T_r = T_c$ or $\rho_r = \rho_c$ is lifted, the artifact disappears. In view of the outlines in section 2 the artifact is irrelevant for this work. Oversized data sets should only be used for assessments of stability and extrapolation behavior. Although the correlation results for the SW_{12} and S_{10} FEOS are by no means gross outliers, we do not include the direct correlations using the $D = 705$ data set in the following discussion.

The emerging critical points from data at only homogeneous states are absolutely realistic for all FEOS correlations under all fit conditions. Across Table 2 the critical temperature varies within $1.077 < T_c < 1.093$. Approximately, $T_c \approx 1.085 \pm 0.008$. No case deviates by more than 1% from the estimated value 1.080 from molecular simulation. Similarly, the critical pressure varies within $0.096 < p_c < 0.104$, or approximately $p_c \approx 0.100 \pm 0.004$. Again, all cases agree within 1% with the estimated value 0.097 from molecular simulation. The critical density is least stable across Table 2 and varies within $0.294 < \rho_c < 0.360$. The uncertainty is up to 10% relative to the estimated value 0.318 from molecular simulation. It becomes evident in section 6.2, however, that molecular simulation faces similar problems. As is, critical compressibility factors vary within $Z_c \approx 0.280 \pm 0.034$. Again, the uncertainty is up to 10% relative to the estimated value 0.282 from molecular simulation.

The Boyle and Joule-Thomson inversion temperature at zero density vary within $2.63 < T_B < 2.89$ and $4.85 < T_{JT} < 5.26$, or approximately $T_B \approx 2.76 \pm 0.13$ and $T_{JT} \approx 5.11 \pm 0.25$. Across Table 2, the maximum deviation from the exact values 2.81 and 5.26 is about 8%.

Table 2 demonstrates shrinking the data set from $M = 705 \rightarrow 481 \rightarrow 271 \rightarrow 101$. Fit quality is assessed by eq. (9) with p, e^r as $P = 2$ properties x_{pm}. The deviation σ_{2M} assesses the quality of the FEOS correlation with respect to the data set used for the fit. The deviation σ_{2D} assesses the quality of the FEOS correlation with respect to a larger data set. In that case, $P(D - M)$ FEOS data are outside the fit margins representing extrapolations. Therefore, σ_{2D} is used as a measure for relative stability.

As mentioned above, the margins for $D = 481$ limit an extended fluid range for technical applications, whereas the margins for $D = 705$ serve as an extreme test. Numerical values for σ's certainly depend on unknown peculiarities of the data sets. We therefore attempt to crop out only trends from Table 2 for decreasing M by data set shrinking. As to be expected, the deviation σ_{2M} slightly decreases for all FEOS. Also, both $\sigma_{2,481}$ and $\sigma_{2,705}$ increase for all FEOS. We believe that σ_{2M} in Table 2 does not allow for a clear ranking of the FEOS correlations concerning reproduction of p and e^r. Given that all FEOS originate from sophisticated optimization procedures, the result is surprising because one would expect the most flexible FEOS (SE_{14}) to perform better than the least flexible FEOS (S_{10}). Both deviations $\sigma_{2,481}$ and $\sigma_{2,705}$ clearly reveal that the S_{10} FEOS is most stable, in accord with what was found for real compounds [22]. The SW_{12} FEOS is clearly more stable than its polar counterpart SW^p_{12}. As expected, due to its increased length the SE_{14} FEOS is significantly less stable than SW_{12}.

Data set thinning was performed as $M = 271 \rightarrow 22$. Besides one outlier, both $\sigma_{2,481}$ and $\sigma_{2,705}$ are roughly independent of M for all FEOS, which may be plausible but by no means obvious. The observation is in accord with Span's thinning experiment for methane [22]. Apparently, using generalized FEOS correlations, data sets as small as some 20 state points are perfectly acceptable for orientations if nothing is known about a fluid. Comparing the generalized FEOS correlations against each other leads to the same conclusions as above: The S_{10} FEOS is clearly the most stable correlation followed by SW_{12}. The SW^p_{12} and SE_{14} FEOS are less stable.

In summary, Table 2 shows that drastic changes in fitting conditions cause little response in the outcome. In general, the resulting critical points appear to be within the uncertainties quoted in section 6.2. The SW^p_{12} FEOS correlation is clearly inferior to the SW_{12} FEOS correlation, as it should. The

SE_{14} FEOS correlation is clearly inferior to both the SW_{12} and S_{10} FEOS correlations, despite its superior flexibility. From the general considerations of this section it appears that the S_{10} FEOS as the shortest generalized FEOS correlation performs best for the LJTS model fluid.

In the following, thermodynamic properties at state points of the original data set are recomputed from an established FEOS correlation by the inverses of eqs. (8a)

$$p = (\delta\alpha^{\mathrm{r}}_{01} + 1)\,\delta\tau^{-1}\,T_{\mathrm{r}}\rho_{\mathrm{r}}\,, \quad e^{\mathrm{r}} = \alpha^{\mathrm{r}}_{10}\,T_{\mathrm{r}}\,, \quad \left(\frac{\partial e^{\mathrm{r}}}{\partial v}\right)_T = -\alpha^{\mathrm{r}}_{11}\,\delta^2\,T_{\mathrm{r}}\rho_{\mathrm{r}}\,, \quad c^{\mathrm{r}}_v = -\alpha^{\mathrm{r}}_{20}\,\tau^2\,. \tag{10a}$$

The derivative $(\partial e^{\mathrm{r}}/\partial v)_T$ is related to the probably more familiar thermal pressure coefficient γ_v [28] through

$$\gamma_v \equiv \left(\frac{\partial p}{\partial T}\right)_v = \frac{1}{T}\left[p - \frac{1}{\rho}\left(\frac{\partial e^{\mathrm{r}}}{\partial v}\right)_T\right] = [1 + \delta\,(\alpha^{\mathrm{r}}_{01} - \tau\alpha^{\mathrm{r}}_{11})]\,\delta\,\rho_{\mathrm{r}}\,, \tag{10b}$$

which describes slopes of isochores in a p, T diagram and is used in section 6.2.

6.1 Homogeneous states

We now turn to a more detailed analysis of the four generalized FEOS correlations. The discussion in sections 2 and 6 supports use of eqs. (8) with α_{01} and α_{10} at $D = 271$ or $D = 481$ state points for the establishment of fit parameters n_i in eq. (3) according to Table 1. The iteration procedure outlined in section 5 yields the parameters in Table 3 so that the reducing state point $(T_{\mathrm{r}}, \rho_{\mathrm{r}})$ equals the *a posteriori* critical state point from the FEOS correlation $(T_{\mathrm{c}}, \rho_{\mathrm{c}})$.

Table 4 displays an average weighted deviation from eq. (9) resolved individually for p, e^{r}, $(\partial e^{\mathrm{r}}/\partial v)_T$, and c^{r}_v. If the FEOS is determined from the data sets $D = 271$ or $D = 481$ with only p and e^{r}, the S_{10} FEOS performs best for all properties, with SW_{12} second, SW^{p}_{12} third, and SE_{14} fourth. In general, the more detailed results here confirm those in section 6. Extrapolation behavior is clearly best for the shortest correlation (S_{10}) and clearly worst for the longest correlation (SE_{14}). Interpolation behavior of the shortest correlation, on the other hand, is not necessarily inferior to the longer ones. Only for pressure and internal energy the ranking is not as obvious as above. For the derivative properties $(\partial e^{\mathrm{r}}/\partial v)_T$ and c^{r}_v, the superiority of S_{10} pertains.

From the results so far it appears that internal energy is probably that property least satisfactorily reproduced by all FEOS correlations. This is not surprising because e^{r} is not directly accessible in laboratory experiments with which all FEOS correlations were optimized. Thermal pressure coefficients γ_v involving $(\partial e^{\mathrm{r}}/\partial v)_T$ according to eq. (10b), on the other hand, are not difficult to establish from accurate $p\rho T$ data. Likewise, heat capacities c_v are also directly accessible in the laboratory, although with diminished experimental accuracy. It is therefore obvious that among the properties available here from molecular simulation, internal energy e^{r} and isochoric heat capacity c^{r}_v are predominant for targeted improvements of generalized FEOS correlations.

Figure 2 shows deviations in pressure. If the data set with $D = 271$ state points is used for the fits all FEOS yield deviations in the region of extrapolation. In all cases the predicted pressures are too low at high temperature and too high at low temperature. The low density region is reproduced accurately throughout. The trend pertains if the data set with $D = 481$ is used, however the uncertainties are significantly reduced in all cases. It is clear from this comparison that the correlations become less accurate as soon as the absolute pressure margin of the data set is surpassed. This observation suggests that pressure margins larger than the projected coverage of state regions should be used. Since the low density low pressure region appears to be easy to correlate [22, Sec. 3.1.4], it could very well be that our distribution of state points is unfortunate: At least for pressure correlations the low density region should probably be thinned relative to the high density high pressure regions.

The residual internal energy is analyzed in Figure 3. The behavior of the FEOS is more complicated than for pressure. Positive and negative deviations from the molecular simulation results take multiple turns across the T, ρ plane predominantly along T, not along ρ. These variations are different for different correlations. Using the data set $D = 271$, the predicted residual internal energies are not negative enough. These deviations set in less abruptly than for pressure. In general, positive and negative deviations do not differ much in magnitude. The low density region for accurate correlations

is significantly smaller than for pressure correlations. Using the data set $D = 481$, the uncertainties become significantly smaller for SW_{12}, SW^{p}_{12}, and SE_{14}. Regions of previous negative deviations may be turned into regions of positive deviations and vice versa. Curiously, neither improvement nor change of behavior is observed for the S_{10} FEOS. We favor this correlation because it is clearly seen that the average weighted deviations in Table 4 come from a relatively small part of the phase diagram at high density and low temperature. Furthermore, the low density region is reproduced accurately over a much larger range than for the other FEOS, which supports the statement made for pressure with respect to targeted distributions of molecular simulation points in the T, ρ plane. Overall, residual internal energy appears to be much more difficult to correlate than pressure. Alternating signs of deviations along T signals potential problems for the correlation of heat capacities, as will be seen below.

Figure 4 shows a comparison of the volume derivative of the residual internal energy, which we call $\gamma^{r}_{T} \equiv (\partial e^{r}/\partial v)_{T}$. The property is related to the isochoric pressure coefficient $\gamma_v \equiv (\partial p/\partial T)_v$ through eq. (10b). Note that γ^{r}_{T} was not used in the fits of this section and is therefore a prediction at all state points. The behavior of the FEOS predictions is similar as for pressure. Using the data set $D = 271$, the correlation values are too low for high temperatures and too high for low temperatures beyond the pressure margin in Table 2. The low density region is accurately correlated. Again, the S_{10} correlation performs outstandingly. Using the data set $D = 481$, changes the results only marginally for SW^{p}_{12} and SE_{14} by introducing some positive deviations at supercritical densities and low temperatures. The SW_{12} FEOS, however, develops a strong positive peak at those conditions. The S_{10} FEOS is virtually unchanged and behaves best. In general, it appears that γ^{r}_{T} it not a serious challenge for any of the FEOS. This can be understood from the fact that isochores in a p, T diagram are close to linear, irrespective density [28]. The results suggest that adding γ^{r}_{T} to multiproperty fits may not yield significant correlation improvements.

The residual isochoric heat capacity $c^{r}_{v} \equiv (\partial e^{r}/\partial T)_v$ is illustrated in Figure 5. As another second order derivative property it was not used in the fits of this section. From the above discussion of the residual internal energy, correlation problems are anticipated. It is clearly seen that the largest deviations occur in the vicinity of the vapor-liquid phase boundary. In general, the correlations predict values significantly higher than the molecular simulation results. Those deviations peak at the critical point, fall off rapidly with increasing temperature, and slowly with density tracing out a bell shaped curve. At high density and low temperature strong positive deviations may develop. For supercritical temperatures the predictions are too high throughout. As for residual internal energy, alternating signs for deviations may be observed along isochores. The data set $D = 271$ increases deviations continuously beyond the pressure margins of Table 4. For c^{r}_{v} the use of data set $D = 481$ induces very little improvement.

As to the S_{10} FEOS: The size of the data set has no effect on the correlation, it performs well under all fit conditions. Whereas beyond slightly supercritical temperatures the predictions are very good, the behavior detoriates around the critical point. In general, it is confirmed that group three FEOS are not designed to reproduce neither the immediate nor the extended critical region. In section 6.4 we investigate the effect of adding c^{r}_{v} to the multiproperty fits.

Figures 2 to 5 show absolute rather than relative deviations for all properties for the following reason. Unlike multiple equipments in the laboratory, molecular simulation emulates one single virtual equipment, which can not be technologically fine-tuned for certain experimental circumstances. For example, pressures in the dense liquid state vary over orders of magnitude, whereas molecular simulation uncertainties are essentially constant, so that relative errors would obscure FEOS correlation assessments in such cases.

This work is based on correlation experience with real compounds. We therefore revisit the accuracy requirements for technical grade FEOS correlations in section 2. Pressure deviations $\Delta p(T, \rho) = p^{ms} - p^{FEOS}$ reported in Figure 2 are converted into density deviations $\Delta\rho(T, p) = \rho^{ms} - \rho^{FEOS}$ by propagating state points along isotherms from the FEOS correlation until $p^{FEOS} = p^{ms} = p$. The shift in density is then considered to be $\Delta\rho(T, p)$. Doing so, density deviation requirements stated in section 2 are essentially met throughout the fluid range by all FEOS correlations. Outliers occur around the critical point, which was intentionally neglected for the original optimization of technical grade quality of FEOS correlations.

In summary, the results of this section reveal that the S_{10} FEOS is not only more stable than

SW_{12}, SW^{p}_{12}, and SE_{14}, it is also the overall most accurate correlation for all molecular simulation data considered here, which contradicts Span's findings for real compounds [22, Sec. 6.2.1.1] in this case.

6.2 Vapor-liquid equilibrium

We now investigate vapor-liquid equilibrium (VLE) as it results from the FEOS correlations fitted to $D = 481$ state points in homogeneous regions using only α^{r}_{01} (from pressure p) and α^{r}_{10} (from residual internal energy e^{r}). No predetermined critical point (T_c, ρ_c) is used for the reducing parameters (T_r, ρ_r) in eq. (1). The FEOS parameters are those reported in Table 3. Previous VLE data for the LJTS model fluid are given in references [41, 42, 43, 44, 45, 46, 47, 38]. Here, we add our own updates at states close to the critical point. The results in Table 5 are obtained as in reference [38] with significantly larger system sizes and longer simulation runs.

Figure 6 compares dew and bubble density $\rho_{v,l}$, vapor pressure p_s, and evaporation enthalpy Δh_s from the predictions of the FEOS correlations and directly simulated vapor-liquid equilibrium data of reference [38] and Table 5. $T_h = 1.05 \approx 0.97 T_c$ is a threshold temperature. Below T_h, state of the art molecular simulation yields VLE data with statistical uncertainties within the required accuracy stated in section 2 (0.2% in p_s and ρ_l, 0.4% in ρ_v). Above T_h those requirements may not be strictly maintainable. From Table 5, at $T = 1.076 \approx 0.995 T_c$ simulation uncertainties for dew and bubble density exceed 3 and 1% respectively. Therefore, for a correlation to qualify as a group three FEOS with technical accuracy, it should pass through the errorbars of the simulations. All FEOS considered here do so for $T < T_h$.

We now ponder the fit strategy of section 5 using the critical point established by Vrabec *et al.* [38] as a reference. Figure 7 magnifies the extended critical region displayed in Figure 6. The critical temperature from the FEOS correlations are too high by 1.4% for SW_{12} and SE_{14}, and by 0.8% for SW^{p}_{12} and S_{10}. For orientation, if noble gases or methane are used as representative real compounds [38], such deviations amount to less than 3 K. The critical density from the FEOS correlations is significantly more uncertain. The deviations are 10% (SW_{12}), -7.1% (SW^{p}_{12}), -4.5% (SE_{14}), and -3.5% (S_{10}). It is interesting that, except SW_{12}, the rectilinear diameters from the FEOS correlations miss the critical density from molecular simulation by only ±1%. The larger discrepency at the critical point comes from a sharp bend in either direction. The behavior depends on the numerical values of the reducing point (T_r, ρ_r) in eq. (1) relative to the critical point and is also responsible for the failure of fits enforcing $T_r = T_c$ and $\rho_r = \rho_c$ under extreme conditions in Table 1. In the laboratory the critical density is usually determined by fitting the rectilinear diameter to a straight line for temperatures from 50 to 3 K below T_c [28]. Using methane as a representative, such an interval corresponds to roughly $0.80 < T < 1.06$. As can be seen from Figure 7, application of the method to FEOS correlation with molecular simulation data may entirely miss the probable bend. In fact, we find it necessary to compute VLE from the FEOS closer to the critical point than $0.9999 T_c$ for a proper linearization of the rectilinear diameter beyond the probable bend. Although it is known that the rectilinear diameter may significantly deviate from truely linear behavior for real compounds close to the critical point [48], we are currently unable to provide further comments on this matter. The behavior is also present in the benchmark FEOS correlation for the LJTS model fluid [15].

Vrabec *et al.* [38] have correlated the vapor pressure curve by an empirical 3 parameter model $p_s = p_s(T)$, which visually performs excellently. Such models can be tested against the Clapeyron equation [28]

$$\frac{\mathrm{d}p_s}{\mathrm{d}T} = \frac{\Delta h_s}{T\left(\rho_v^{-1} - \rho_l^{-1}\right)}\,, \quad \text{or} \quad \frac{\mathrm{d}\ln p_s}{\mathrm{d}T^{-1}} = -\frac{T\Delta h_s}{p_s\left(\rho_v^{-1} - \rho_l^{-1}\right)}\,, \tag{11}$$

they must obey. All quantities on the right hand sides are direct molecular simulation results with overall statistical errors determined by the standard error propagation law. Figure 8 reveals that the vapor pressure correlation in reference [38, eq. (3)] is inconsistent with eq. (11). All FEOS correlations considered here remove these inconsistencies. Those results convincingly demonstrate that individual VLE correlations are obsolete once a sophisticated FEOS with built-in thermodynamic consistency is available.

Above findings for the immediate vicinity of the critical point are confirmed: Bends in the rectilinear diameter in Figure 7 have counterparts in bends in the slopes of the vapor pressure curve in Figure 8.

The vapor pressures can be subject to a further thermodynamic consistency test. At the critical point [28]

$$\gamma_\mathrm{s} \equiv \frac{\mathrm{d}p_\mathrm{s}}{\mathrm{d}T} = \left(\frac{\partial p}{\partial T}\right)_v \equiv \gamma_v \,, \quad \text{for} \quad T = T_\mathrm{c} \quad \text{and} \quad \rho = \rho_\mathrm{c} \,. \tag{12}$$

In words, the slope of the vapor pressure curve γ_s must equal the homogeneous thermal pressure coefficient γ_v of eq. (10b). Figure 8 shows five distinct critical points in this context, one from the direct molecular simulations of Vrabec *et al.* [38], and four from the FEOS correlations quantified in Table 5 for $D = 481$. As for the FEOS correlations, the computation of γ_s at the critical point from eq. (11) involves an undetermined 0/0, which requires a proper numerical limiting process. The computation of γ_v from eq. (10b) is straightforward. Eventually, we confirm consistency $\gamma_\mathrm{s} = \gamma_v$ in eq. (12) with the specific results 0.624 (SW_{12}), 0.503 ($\mathrm{SW}^\mathrm{p}_{12}$), 0.532 ($\mathrm{SE}_{14}$), and 0.545 ($\mathrm{S}_{10}$) for the distinct critical points in Table 3. If one were to accept the critical point from direct molecular simulation [38] ($T_\mathrm{c} = 1.078$, $\rho_\mathrm{c} = 0.319$, $\gamma_\mathrm{s} = 0.450$) as true, γ_v from the FEOS correlations is 0.555 (SW_{12}), 0.532 ($\mathrm{SW}^\mathrm{p}_{12}$), 0.554 ($\mathrm{SE}_{14}$), and 0.560 ($\mathrm{S}_{10}$), inconsistent with eq. (12) by about 20% in all cases.

In summary, the results of this section numerically confirm internal consistency of all FEOS correlations used here. It shows that group three FEOS are not designed to describe the immediate vicinity of the critical point accurately. Sudden bends in the rectilinear diameter and the slope of the vapor pressure curve are possible. These bends may very well be in violation of physical behavior, however, they still satisfy thermodynamic consistency.

6.3 Virial coefficients and ideal curves

The virial EOS

$$p/\rho T = 1 + B_2(T)\rho + B_3(T)\rho^2 + \cdots \tag{13a}$$

is a meaningful power expansion of pressure about the density limit $\rho \to 0$. It defines the n^th virial coefficient $B_n(T)$ as

$$B_n(T) = \lim_{\rho=0} \frac{\partial^{n-2}}{\partial \rho^{n-2}} \left(\frac{p/\rho T - 1}{\rho}\right)_T = \rho_\mathrm{r}^{-(n-1)} \lim_{\delta=0} \alpha^\mathrm{r}_{0,n-1} \,. \tag{13b}$$

Virial coefficients are molecular properties, which can be rigorously computed. For pair potentials of the form $u = u(r_{ij})$ [49, 50]

$$B_2(T) = -2\pi \int_0^\infty f(r_{12}) r_{12}^2 \, \mathrm{d}r_{12} \,, \tag{14a}$$

$$B_3(T) = -\frac{8}{3}\pi^2 \int_0^\infty \int_0^\infty \int_{-1}^1 f(r_{12}) f(r_{13}) f(r_{23}) \, r_{12}^2 r_{13}^2 \, \mathrm{d}\cos\alpha \, \mathrm{d}r_{13} \, \mathrm{d}r_{12} \,, \tag{14b}$$

$$\text{with} \qquad f(r_{ij}) \equiv \exp\left[u(r_{ij})/T\right] - 1 \quad \text{and} \quad r_{23}^2 = r_{12}^2 - 2r_{12}r_{13}\cos\alpha + r_{13}^2 \,, \tag{14c}$$

with α being the angle between r_{12} and r_{13} and no further refinement for symmetries of the problem. The integrals are solved numerically.

Figure 9 shows comparisons for second and third virial coefficients. Obviously, all empirical FEOS correlations can predict the second virial coefficient. The correlations begin to fail quantitatively for the third virial coefficient. Higher virial coefficients can not be reproduced by the generalized FEOS correlations considered here. However, virial coefficients are of no practical importance if sophisticated FEOS correlations are available. It would therefore be purely academical to discuss virial coefficients beyond the second.

Experts in the field of thermodynamic data correlation demand from FEOS correlation realistic reproduction of so-called ideal curves [51, 22]. Such curves relate to properties of a compound as if at vanishing density, the ideal gas state. In statistical mechanics, ideal curves are univocally accessible in the limit of zero density for any given molecular interaction model with arbitrary numerical accuracy. Here we consider two such state points:

(1) The Boyle temperature $T_{\rm B}$ tags the state point at zero density, where the second virial coefficient $B_2(T)$ in the virial EOS eq. (13b) equals zero. It is the origin of both the Boyle curve and the ideal curve [22].

(2) The Joule-Thomson inversion temperature $T_{\rm JT}$ tags the state point at zero density, where the Joule-Thomson coefficient $\mu_{\rm JT} \equiv (\partial T/\partial p)_h$ equals zero. It is the origin of the Joule-Thomson inversion curve [22].

The conditions are therefore

$$B_2(T = T_{\rm B}) = 0\,, \quad \text{and} \quad \lim_{\rho=0} \mu_{\rm JT}(\rho, T = T_{\rm JT}) = 0\,. \tag{15a}$$

Such conditions involve no more than $p\rho T$ data, as can be seen through eq. (13b) and the thermodynamic identities

$$\lim_{\rho=0} \mu_{\rm JT}(\rho, T) = -\frac{{\rm d}[B_2(T)/T]}{{\rm d}T^{-1}} = T\frac{{\rm d}B_2(T)}{{\rm d}T} - B_2(T)\,. \tag{15b}$$

In the laboratory, the above conditions are derived properties (impossible to measure directly). In statistical mechanics they constitute $p\rho T$ data, albeit without statistical errors. The rigorous determination of $T_{\rm B}$ and $T_{\rm JT}$ for a variety of molecular interaction models is described in references [49, 52, 53]. In summary, the conditions in eq. (15a) are fullfilled, with eq. (4), if

$$\int_0^\infty [\exp[-u(r)/T] - 1]\, r^2\, {\rm d}r = 0\,, \quad \text{and} \quad \int_0^\infty [(1 - u(r)/T)\exp[-u(r)/T] - 1]\, r^2\, {\rm d}r = 0\,, \tag{15c}$$

where it is to be remembered that all quantities are reduced (starred) quantities. We obtain $T_{\rm B} = 2.806$ and $T_{\rm JT} = 5.256$. Using the critical temperature $T_{\rm c} = 1.082$, it is interesting that the ratios $T_{\rm JT} : T_{\rm B} : T_{\rm c} = 4.8 : 2.6 : 1$ are consistent with what was found for a variety of other models [52, 53] and real compounds [54]. In terms of FEOS correlations the above discussed state points are determined by

$$\delta = 0, \tau = \tau_{\rm B} :\ \lim_{\delta=0} \alpha^{\rm r}_{01} = 0\ , \quad \text{and} \quad \delta = 0, \tau = \tau_{\rm JT} :\ \lim_{\delta=0} (\alpha^{\rm r}_{01} + \delta\alpha^{\rm r}_{02} + \tau\alpha^{\rm r}_{11}) = 0\,. \tag{16}$$

The results of the above outline are displayed in Figure 10 with parameters from $D = 481$ state points, as specified in Table 3. The Joule-Thomson inversion curve is presented in three-dimensional $p\rho T$-space. Clearly, from low temperatures to the maximum, the Joule-Thomson inversion curve is predicted almost identically by all FEOS correlations. Beyond the maximum, deviations occur and culminate only in the p, T-projection at very low density. In summary, the Joule-Thomson inversion curve, as computed from the FEOS correlations, appears to not violate established behavior, as other correlations may [22, Secs. 4.6.3 and 6.2.1.1]. In this work, we did not attempt to verify the predicted Joule-Thomson inversion curves by molecular simulation, as current standards constitute a major undertaking to do so [55]. However, a rigorous measuring prescription for the Joule-Thomson coefficient in molecular NVT simulation has been devised recently [37, 56]. Therefore, direct checks of the predictions in Figure 10 are possible in principle. We will implement the measuring prescription in $ms2$ [36]. Here, Joule-Thomson inversion curves are predicted through FEOS correlation only. If the four correlations are considered to be independent prediction models, we state from Table 6 that the Joule-Thomson inversion curve has a maximum most likely to occur at $T_{\rm m} = 2.42 \pm 0.08$, $p_{\rm m} = 1.14 \pm 0.01$, $\rho_{\rm m} = 0.38 \pm 0.01$, and an intersection with the bubble line most likely to occur at $T_{\rm s} = 0.878 \pm 0.003$, $p_{\rm s} = 0.0270 \pm 0.0005$, $\rho_{\rm l} = 0.678 \pm 0.003$. Using similar arguments for a prediction of the Joule-Thomson inversion temperature at zero density from FEOS correlations yields $T_{\rm JT} = 5.16 \pm 0.23$, consistent with the exact value of 5.256.

6.4 Effects of increasing the number of fit properties

The previous sections were concerned with current standards of using pressure and internal energy for thermodynamic data correlation. We now turn to addition of thermodynamic properties beyond current standards. The last sections confirm that, using pressure p and residual internal energy $e^{\rm r}$ only, all FEOS correlations represent $p\rho T$, $e^{\rm r}$ data and their temperature and density derivatives well. One may anticipate that additional thermodynamic properties may distort the fits. Agreements with

$(\partial e^{\mathrm{r}}/\partial v)_T$ and $c_v^{\mathrm{r}} \equiv (\partial e^{\mathrm{r}}/\partial T)_v$ will become better if they are included, whereas agreements with p and e^{r} may worsen. The inclusion of properties not accessible in the laboratory have, of course, never been analyzed for usefulness in FEOS correlation. To do so, we start from current standards using the data set $D = 481$ outlined in Table 2 and create the four scenarios in Table 7:

(1) Use $\alpha_{01}^{\mathrm{r}} \propto p$ and $\alpha_{10}^{\mathrm{r}} \propto e^{\mathrm{r}}$ as outlined in previous sections.

(2) Add $\alpha_{11}^{\mathrm{r}} \propto (\partial e^{\mathrm{r}}/\partial v)_T$.

(3) Add $\alpha_{20}^{\mathrm{r}} \propto c_v^{\mathrm{r}} \equiv (\partial e^{\mathrm{r}}/\partial T)_v$.

(4) Add α_{11}^{r} and α_{20}^{r} simultaneously.

Several overall weighted deviations according to eq. (9) are used:

(1) $\sigma_{2,481}$: Uses the fit data set for assessment. Quantifies to what extent the p and e^{r} representations by the FEOS correlations worsen by including additional properties.

(2) $\sigma_{4,481}$: Uses the fit data set for assessment. Quantifies to what extent the overall fit quality improves by including additional properties.

(3) $\sigma_{2,705}$: Uses an oversized data set for assessment. Quantifies to what extent the extrapolation behavior of p and e^{r} is worsend by including additional properties.

(4) $\sigma_{4,705}$: Uses an oversized data set for assessment. Quantifies to what extent the overall extrapolation behavior improves by including additional properties.

A horizontal examination of those weighted deviations in Table 7 allows for a clear ranking of the generalized FEOS correlations. As already concluded and outlined in sections 6 and 6.1, the S_{10} FEOS performs best in all scenarios, followed by SW_{12}, $\mathrm{SW}_{12}^{\mathrm{p}}$, and SE_{14}. Again, such ranking does by no means imply failure. We still consider the SE_{14} FEOS a very good correlation, much better than any cubic type EOS could be. We stress again that these FEOS correlations are outcomes of purely mathematical models: No physical concept whatsoever is involved. As molecular thermodynamicists, we find it frustrating albeit amazing how dominantly these models defeat any semi-empirical attempt we were involved in or are aware of.

A vertical examination of Table 7 reveals that inclusion of α_{11}^{r} has no effect. Inclusion of α_{20}^{r}, however, does have an effect on the correlations, which we now discuss using the above weighted deviations. $\sigma_{2,481}$ increases by a factor of roughly 2. This means that inclusion of α_{20}^{r} worsens the p and/or e^{r} representations for all FEOS correlations. $\sigma_{4,481}$ decreases by a factor of roughly 2. Inclusion of α_{20}^{r} overcompensates the worsening of p and/or e^{r} globally. $\sigma_{2,705}$ increases by a factor of roughly 1.5. This means that inclusion of α_{20}^{r} worsens the p, e^{r} extrapolation (in excess of representation) behavior for all FEOS correlations. $\sigma_{4,705}$ stays about constant, which means that the inclusion of α_{20}^{r} globally compensates the worsening extrapolation behavior for p and e^{r}. All mentioned effects are significantly less pronounced for the S_{10} FEOS, which is another advocacy for its superior stability. Table 7 also contains the critical points, Boyle, and Joule-Thomson inversion temperatures at zero density.

If α_{20}^{r} is added, the overall accuracy decreases. The finding is probably least surprising in view of eq. (10b), showing that α_{11}^{r} solely depends on $p\rho T$ data, accurately accessible in the laboratory, whereas α_{20}^{r} is not so. Calorimetric laboratory experiments do not only exhibit larger errors than $p\rho T$ experiments, they are also more expensive to perform. Simply, much less experimental data are available for caloric than for thermal thermodynamic properties. All FEOS correlations were optimized using laboratory data. Therefore, if properties correlate less satisfactorily, it should be α_{10}^{r} and α_{20}^{r}, which appears to be the case here.

7 Conclusions

Our compound specific and fully optimized benchmark FEOS correlation for the LJTS model fluid with 21 terms [15] is more accurate than any of the correlations considered here. However, in this work the

emphasis is on generalization. We wish to rationalize molecular simulation data routinely, possibly on the fly. The benchmark FEOS was optimized with the $D = 705$ data set using $\alpha^{\rm r}_{01}, \alpha^{\rm r}_{10}, \alpha^{\rm r}_{11}, \alpha^{\rm r}_{20}$. Neither reducing the data set nor effects of the nature of thermodynamic properties included in the fits were investigated in that work. Here, we have exhausted generalized fully empirical correlation possibilities of molecular simulation data based on established evidence from real compounds.

It is confirmed through this work that molecular simulation data can be efficiently correlated by FEOS. In particular, correlations can be accomplished with low parameter FEOS exhibiting technical accuracy. Whereas empirical data correlation is compound specific, it can still be generalized to classes of compounds by employing state-of-the-art multiproperty correlation strategies. In this work we examined four particular FEOS correlations developed for the classes of non-polar and polar compounds from real laboratory experiments, here applied to molecular simulation data. The LJTS model fluid is simple and non-polar. If the concept of generalized FEOS correlation based on real laboratory evidence does carry over to molecular simulation data, then it should be the generalized correlations for polar compounds to rank last in the present case: They do.

The strategy advocated here is meant as a generalized supplement to large scale molecular simulations of molecular interaction models for fluid systems. Usually, nothing is known about details of the phase behavior of models. In particular, for the purpose at hand, possible two-phase regions involving fluid and solid states must be identifiable. Based on the experience gained in this work, there is no need to identify vapor-liquid, vapor-solid, or liquid-solid phase equilibrium *a priori*. All FEOS correlations considered here will signal the presence of two phases by gross fit outliers. The overall fit procedure will then consist of iterations removing unwanted data points.

The use of constraints [39] is popular in thermodynamic correlations. They pin a FEOS correlation to exact predetermined values. As such, they have a pronounced effect on overall performance and must not be used excessively. In reference FEOS correlations, an accurate knowledge of the critical point is always used as a constraint to enforce $\tau_{\rm c} = \delta_{\rm c} = 1$, as in eq. (1). As indicated around Table 5, critical points for model fluids update as computing power increases. Our own update from 2006 [38] suggests a conservative estimate of uncertainties $\Delta_{T_{\rm c}} \approx \Delta_{\rho_{\rm c}} \approx \Delta_{p_{\rm c}} > \pm 0.01$, which is higher than laboratory based estimates. Therefore, unlike for real compounds, we would not use estimated critical properties as fit constraints if a ciritical point can not be established more accurate than 0.1 percent in both temperature and pressure, and 1 percent in density. All is not the case to date for molecular simulation data. Other state points, such as in eq. (16), can be computed for molecular models with arbitrary accuracy, so that they could serve as constraints. Here, Boyle and Joule-Thomson inversion temperatures at zero density are sufficiently represented without constraints. Use as constraints would not enhance practical benefits.

For all four generalized FEOS correlations considered in this work, stability criteria, as defined by Span [22], are fullfilled, but to varying degree: Low parameter FEOS correlations appear to tolerate extremely small molecular simulation data sets. Some 700 original homogeneous state points cover extreme conditions. Reduction in various scenarios to some 20 homogeneous state points, covering mildly ambient conditions, does not alter the quality of the resulting FEOS correlation discernibly. Currently, we are not in a position to project far reaching consequences onto other model fluids.

FEOS correlation has a built-in guarantee of thermodynamic consistency. Vapor-liquid equilibrium correlations on the other hand, as in reference [38], are most likely subject to inconsistencies. Corresponding findings for the LJTS fluid using FEOS correlation are therefore no surprise. As outlined by Span [22], vapor-liquid equilibrium correlations have no rigorous meaning other than providing starting values for iterations in case an accurate FEOS correlation for a compound is available, which is confirmed here.

We suggest that fully empirical FEOS correlations be considered an unavoidable complement to molecular simulation for practical purposes. The four alternatives considered here cover non-polar and polar compounds. We feel that those choices can be routinely and confidentially used for molecular simulation data reduction. One of them will perform better than others for particular cases. In the present case, for a simple non-polar model fluid, the non-polar versions $\rm S_{10}$ and $\rm SW_{12}$ performed best, as should be. Recent requests to make molecular simulation a more mainstream tool in engineering [27] are definitely satisfied by the results of this work.

Thermodynamic correlation of real laboratory data and molecular simulation data differ in the underlying uncertainties. Whereas thermal ($p\rho T$) data have lower uncertainties in the real laboratory,

residual caloric data have much lower uncertainties if measured for a model system in molecular simulation. Weighted deviations eq. (9) of molecular simulation data (for example Tables 2, 4, 7) are then significantly larger than real laboratory counterparts (for example [22, sec. 6.2]) simply because of lower associated uncertainties $\Delta_{x_{pm}}$. Scenario (2) in section 5 applies to most of the uncertainties reported in this work: Molecular simulation uncertainties are not reported too low, they are low indeed. Increased correlation deviations for residual internal energy e^{r} of all generalized FEOS models are due to extraordinary low molecular simulation uncertainties. Such numbers are not alarming because e^{r} can not be measured in the real laboratory directly, and has therefore never been used for correlation assessment. In the context of this work it appears that fully empirical generalized FEOS correlation would benefit from a systematic investigation of well-defined model systems in molecular simulation.

Acknowledgement
We thank a reviewer for helpful comments around eq. (9). Gabriela Guevara-Carrion provided the molecular simulation results. Monika Thol provided all numbers related to the benchmark FEOS [15]. Part of this work was sponsored by Deutsche Forschungsgemeinschaft under grant VR6/4-2. Computational support was given by the High Performance Computing Center Stuttgart (HLRS) under grant MMHBF2.

References

[1] I.R. McDonald and K. Singer, Mol. Phys. **23** (1), 29 (1972). Erratum: Mol. Phys. **24** (2), 464 (1972).

[2] J.J. Nicolas, K.E. Gubbins, W.B. Streett and D.J. Tildesley, Mol. Phys. **37** (5), 1429 (1979).

[3] M. Luckas and K. Lucas, Fluid Phase Equilibr. **45** (1), 7 (1989).

[4] J.K. Johnson, J.A. Zollweg and K.E. Gubbins, Mol. Phys. **78** (3), 591 (1993).

[5] J. Kolafa and I. Nezbeda, Fluid Phase Equilibr. **100** (0), 1 (1994).

[6] M. Mecke, A. Müller, J. Winkelmann, J. Vrabec, J. Fischer, R. Span and W. Wagner, Int. J. Thermophys. **17** (2), 391 (1996). Erratum: Int. J. Thermophys. **19** (5), 1493 (1998).

[7] M. Mecke, A. Müller, J. Winkelmann and J. Fischer, Int. J. Thermophys. **18** (3), 683 (1997).

[8] C. Kriebel, M. Mecke, J. Winkelmann, J. Vrabec and J. Fischer, Fluid Phase Equilibr. **142** (1), 15 (1998).

[9] M.A. Van der Hoef, J. Chem. Phys. **113** (18), 8142 (2000).

[10] M. Lisal, K. Aim, M. Mecke and J. Fischer, Int. J. Thermophys. **25** (1), 159 (2004).

[11] J. Gross, AIChE J. **51** (9), 2556 (2005).

[12] J. Gross and J. Vrabec, AIChE J. **52** (3), 1194 (2006).

[13] J. Vrabec and J. Gross, J. Phys. Chem. B **112** (1), 51 (2008).

[14] H.-O. May and P. Mausbach, Phys. Rev. E **85** (3), 031201 (2012).

[15] M. Thol, G. Rutkai, R. Span, J. Vrabec and R. Lustig, Int. J. Thermophys. **36** (1), (2015).

[16] M. Thol, G. Rutkai, A. Köster, M. Kortmann, R. Span and J. Vrabec, Chem. Eng. Sci. **121** (0), 87 (2015).

[17] C.G. Gray and K.E. Gubbins, *Theory of Molecular Fluids 1: Fundamentals* (Oxford University Press, Oxford, 1984).

[18] C.G. Gray, K.E. Gubbins and C.G. Joslin, *Theory of Molecular Fluids 2: Applications* (Oxford University Press, Oxford, 2011).

[19] T. Boublik and I. Nezbeda, Coll. Czech. Chem. Comm. **51** (11), 2301 (1986).

[20] G. Rutkai, M. Thol, R. Lustig, R. Span and J. Vrabec, J. Chem. Phys. **139** (4), 041102 (2013).

[21] R. Tillner-Roth, *Fundamental Equations of State* (Shaker, Aachen, 1998).

[22] R. Span, *Multiparameter Equations of State* (Springer, Berlin, 2000).

[23] J.M. Prausnitz, R.N. Lichtenthaler and E.G. de Azevedo, *Molecular Thermodynamics of Fluid-phase Equilibria*, 3rd ed. (Prentice Hall, Upper Saddle River, 1999).

[24] M. Benedict, G.B. Webb and L.C. Rubin, J. Chem. Phys. **8** (4), 334 (1940).

[25] K.E. Gubbins and N. Quirke (Editors), *Molecular Simulation and Industrial Applications* (Gordon and Breach, Amsterdam, 1996).

[26] A.H. Harvey and A. Laesecke, Chem. Eng. Prog. **98** (2), 34 (2002).

[27] E.J. Maginn, AIChE J. **55** (6), 1304 (2009).

[28] J.S. Rowlinson and F.L. Swinton, *Liquids and Liquid Mixtures*, 3rd ed. (Butterworths, London, 1982).

[29] R. Span and W. Wagner, Int. J. Thermophys. **24** (1), 1 (2003).

[30] R. Span and W. Wagner, Int. J. Thermophys. **24** (1), 41 (2003).

[31] L. Sun and J.F. Ely, Fluid Phase Equilibr. **222** (0), 107 (2004).

[32] K.B. Shubert and J.F. Ely, Int. J. Thermophys. **16** (1), 101 (1995).

[33] E.W. Lemmon and R.T. Jacobsen, J. Phys. Chem. Ref. Data **34** (1), 69 (2005).

[34] H. Flyvbjerg and H.G. Petersen, J. Chem. Phys. **91** (1), 461 (1989).

[35] R. Lustig, J. Chem. Phys. **100** (4), 3068 (1994).

[36] C.W. Glass, S. Reiser, G. Rutkai, S. Deublein, A. Köster, G. Guevara-Carrion, A. Wafai, M. Horsch, M. Bernreuther, T. Windmann, H. Hasse and J. Vrabec, Comp. Phys. Comm. **185** (12), 3302 (2014).

[37] R. Lustig, Mol. Sim. **37** (6), 457 (2011).

[38] J. Vrabec, G.K. Kedia, G. Fuchs and H. Hasse, Mol. Phys. **104** (9), 1509 (2006).

[39] J.G. Hust and R.D. McCarty, Cryogenics **7** (14), 200 (1967).

[40] E.A. Guggenheim, J. Chem. Phys. **13** (7), 253 (1945).

[41] P. Adams and J.R. Henderson, Mol. Phys. **73** (6), 1383 (1991).

[42] B. Smit, J. Chem. Phys. **96** (11), 8639 (1992).

[43] P.J. Camp and M.P. Allen, Mol. Phys. **88** (6), 1459 (1996).

[44] M. Mareschal, M. Baus and R. Lovett, J. Chem. Phys. **106** (2), 645 (1997).

[45] A. Trokhymchuk and J. Alejandre, J. Chem. Phys. **111** (18), 8510 (1999).

[46] W. Shi and J.K. Johnson, Fluid Phase Equilibr. **187** (0), 171 (2001).

[47] D.O. Dunikov, S.P. Malyshenko and V.V. Zhakhovskii, J. Chem. Phys. **115** (14), 6623 (2001).

[48] L.J. Van Poolen, R.T. Jacobsen and M. Jahangiri, Int. J. Thermophys. **7** (3), 513 (1986).

[49] J.O. Hirschfelder, C.F. Curtiss, R.B. Bird, *Molecular Theory of Gases and Liquids* (Wiley, New York, 1954).

[50] K. Lucas, *Applied Statistical Thermodynamics* (Springer, Berlin, 1991).

[51] U.K. Deiters and K.M. De Reuck, Pure App. Chem. **69** (6), 1237 (1997).

[52] A. Friedrich and R. Lustig, J. Chem. Phys. **105** (21), 9597 (1996).

[53] T. Breitenstein and R. Lustig, J. Mol. Liq. **9899** (0), 261 (2002).

[54] J.S. Rowlinson, *T*he Properties of Real Gases. In: *Ecyclopedia of Physics*, edited by S. Flügge (Springer, Berlin, 1958, pp. 1-72).

[55] J. Vrabec, G.K. Kedia and H. Hasse, Cryogenics **45** (4), 253 (2005).

[56] R. Lustig, Mol. Phys. **110** (24), 3041 (2012).

[57] L. Sun and J.F. Ely, Int. J. Thermophys. **26** (3), 705 (2005).

[58] K.R.S. Shaul, A.J. Schultz and D.A. Kofke, Coll. Czech. Chem. Comm. **75** (4), 447 (2010).

#	Span-Wagner (12)				polar Span-Wagner (12)				Sun-Ely (14)				Span (10)			
	p_i	d_i	t_i	i	p_i	d_i	t_i	i	p_i	d_i	t_i	i	p_i	d_i	t_i	i
1 (1)													-	1	$1/8 = 0.125$	1
2 (3)	-	1	$2/8 = 0.250$	1	-	1	$2/8 = 0.250$	1	-	1	$2/8 = 0.250$	2				
3 (2)	-	1	$9/8 = 1.125$	2									-	1	$9/8 = 1.125$	2
4 (2)					-	1	$10/8 = 1.250$	2	-	1	$10/8 = 1.250$	3				
5 (3)	-	1	$12/8 = 1.500$	3	-	1	$12/8 = 1.500$	3	-	1	$12/8 = 1.500$	1				
6 (1)													-	2	$10/8 = 1.250$	3
7 (2)	-	2	$11/8 = 1.375$	4					-	2	$11/8 = 1.375$	6				
8 (4)	-	3	$2/8 = 0.250$	5	-	3	$2/8 = 0.250$	4	-	3	$2/8 = 0.250$	4	-	3	$2/8 = 0.250$	4
9 (3)	-	7	$7/8 = 0.875$	6	-	7	$7/8 = 0.875$	5	-	7	$7/8 = 0.875$	5				
10 (1)													-	8	$6/8 = 0.750$	5
11 (1)									1	1	$0/8 = 0.000$	7				
12 (2)					1	1	$19/8 = 2.375$	6	1	1	$19/8 = 2.375$	8				
13 (2)	1	2	$5/8 = 0.625$	7									1	2	$5/8 = 0.625$	6
14 (2)					1	2	$16/8 = 2.000$	7	1	2	$16/8 = 2.000$	9				
15 (1)													1	3	$16/8 = 2.000$	7
16 (1)	1	5	$14/8 = 1.750$	8												
17 (2)					1	5	$17/8 = 2.125$	8	1	5	$17/8 = 2.125$	10				
18 (2)					2	1	$28/8 = 3.500$	9	2	1	$28/8 = 3.500$	11				
19 (1)	2	1	$29/8 = 3.625$	9												
20 (1)													2	1	$33/8 = 4.125$	8
21 (2)					2	1	$52/8 = 6.500$	10	2	1	$52/8 = 6.500$	12				
22 (1)	2	4	$29/8 = 3.625$	10												
23 (1)													2	4	$33/8 = 4.125$	9
24 (2)					2	4	$38/8 = 4.750$	11	2	4	$38/8 = 4.750$	13				
25 (2)					3	2	$25/2 = 12.50$	12	3	2	$25/2 = 12.50$	14				
26 (1)	3	3	$29/2 = 14.50$	11												
27 (1)													3	3	$34/2 = 17.00$	10
28 (1)	3	4	$24/2 = 12.00$	12												

Table 1: Comparison of the Span-Wagner and Sun-Ely FEOS, referred to in this paper as SW_{12}, SW^{P}_{12}, SE_{14}, and S_{10}. All FEOS are of MBWR type and have the specific form of eq. (3) with $\gamma_i = 1$. Labels i refer to the labels in the original sources [22, eqs. (6.12), (6.13), (7.20), (7.21), Table 7] and [31, eq. (16), Table 1]. The first column numbers all 28 basis functions shared by the four correlations, with their occurences in parantheses. The sorting is with ascending first t_i, second d_i, and third p_i. It is clearly seen through this representation, that the three Span-Wagner FEOS (SW_{12}, SW^{P}_{12}, and S_{10}) are largely independent developments, because they have little basis functions in common. These authors initially offered their genetic algorithm a bank of basis functions with 584 members for selection [22]. The Sun-Ely FEOS (SE_{14}) was selected out of some bank of basis functions not further specified by a simulated annealing strategy [31, 57]. Since the two optimization strategies are entirely unrelated, it is puzzling that the resulting SE_{14} correlation is an almost perfect linear combination of SW_{12} and SW^{P}_{12}: Only basis function 11 is not contained in either SW_{12} or SW^{P}_{12}.

T_m	ρ_m	p_m	M	σ_{2M}	$\sigma_{2,481}$	$\sigma_{2,705}$	$T_\mathrm{r} = T_\mathrm{c}$	$\rho_\mathrm{r} = \rho_\mathrm{c}$	p_c	Z_c	T_B	T_JT
11.0	0.94	6.8	705	5.4		5.4	1.086	0.319	0.101	0.292	2.78	5.25
11.0	0.94	6.8	705	22.8		22.8	1.106	0.360	0.113	0.284	2.81	5.27
							overall iteration failed for $\mathrm{SW}_{12}^\mathrm{p}$ and SE_{14}					
				16.1		16.1	1.084	0.322	0.100	0.288	2.81	5.30
5.0	0.85	2.0	481	52	52	158	1.093	0.350	0.104	0.279	2.82	5.26
				47	47	209	1.086	0.296	0.099	0.308	2.68	4.93
				57	57	232	1.093	0.305	0.102	0.307	2.78	5.12
				57	57	84	1.086	0.308	0.101	0.301	2.84	5.35
2.5	0.85	0.5	271	30	75	233	1.084	0.348	0.100	0.264	2.85	5.29
				26	91	300	1.087	0.316	0.101	0.294	2.71	4.99
				39	153	480	1.086	0.335	0.101	0.277	2.78	5.05
				20	37	80	1.086	0.308	0.101	0.300	2.82	5.31
			22	55	75	222	1.077	0.360	0.096	0.246	2.84	5.28
				68	110	338	1.090	0.324	0.103	0.293	2.73	5.01
				1634	1299	1617	1.081	0.334	0.097	0.269	2.79	5.08
				15	36	106	1.086	0.294	0.100	0.313	2.82	5.32
1.2	0.83	0.2	101	30	98	277	1.082	0.351	0.099	0.260	2.89	5.36
				23	135	389	1.083	0.329	0.099	0.278	2.73	4.98
				7	74	319	1.084	0.329	0.100	0.279	2.63	4.85
				16	60	120	1.081	0.321	0.098	0.282	2.76	5.21

Table 2: FEOS correlation results. The first row presents our fully optimized benchmark correlation of reference [15]. That FEOS was fitted to all available molecular simulation data at $M = 705$ state points. In subsequent rows, that original data set was shrunk under limiting conditions (subscript m) for temperature, density, and pressure as illustrated in Figure 1. The state point margins $T_\mathrm{m} = 5$ and $p_\mathrm{m} = 2$ ($M = 481$) limit technically sensible applications (see section 2). The state point margins $T_\mathrm{m} = 2.5$ and $p_\mathrm{m} = 0.5$ correspond to the range targeted for group three FEOS correlations. Those margins were used for arbitrarily thinning the $M = 271$ data set. Consecutive rows are for the FEOS correlations SW_{12}, $\mathrm{SW}_{12}^\mathrm{p}$, SE_{14}, and S_{10}. Here, only α_{01}^r (from pressure p) and α_{10}^r (from residual internal energy e^r) are used for the fits, so that $P = 2$ in eq. (9) for the fit assessments σ_{2M}, $\sigma_{2,481}$, and $\sigma_{2,705}$ (see text). The critical points emerge from convergence of the overall iteration procedure described in section 5 so that $\tau_\mathrm{c} = \delta_\mathrm{c} = 1$ in all cases. Vrabec *et al.* [38] report for the critical point $T_\mathrm{c} = 1.0779$, $\rho_\mathrm{c} = 0.3190$, $p_\mathrm{c} = 0.0935$, with a resulting critical compressibility factor $Z_\mathrm{c} \equiv p_\mathrm{c}/\rho_\mathrm{c}T_\mathrm{c} = 0.272$. From eqs. (15) the Boyle temperature and Joule-Thomson inversion temperature at zero density are precisely $T_\mathrm{B} = 2.806$ and $T_\mathrm{JT} = 5.256$.

D/i	SW_{12}	$\mathrm{SW}^{\mathrm{p}}_{12}$	SE_{14}	S_{10}
271	$T_\mathrm{r} = T_\mathrm{c} = 1.0837$	$T_\mathrm{r} = T_\mathrm{c} = 1.0873$	$T_\mathrm{r} = T_\mathrm{c} = 1.0858$	$T_\mathrm{r} = T_\mathrm{c} = 1.0863$
	$\rho_\mathrm{r} = \rho_\mathrm{c} = 0.3484$	$\rho_\mathrm{r} = \rho_\mathrm{c} = 0.3164$	$\rho_\mathrm{r} = \rho_\mathrm{c} = 0.3348$	$\rho_\mathrm{r} = \rho_\mathrm{c} = 0.3084$
1	$0.96567442E+00$	$0.85842741E+00$	$0.83936920E+00$	$0.62832230E+00$
2	$-0.27247402E+01$	$-0.30321803E+01$	$-0.21235453E+01$	$-0.16240298E+01$
3	$0.70542114E+00$	$0.10150787E+01$	$-0.23928234E+00$	$-0.56544070E-01$
4	$-0.81497912E-01$	$0.72042750E-01$	$0.11282992E+00$	$0.69371366E-01$
5	$0.10508043E+00$	$0.33024837E-03$	$0.65184407E-01$	$0.71178545E-04$
6	$0.55698055E-03$	$0.36120698E+00$	$0.40999175E-03$	$0.21742890E+00$
7	$0.29208379E+00$	$0.52457088E+00$	$-0.50961391E-02$	$0.10902180E+00$
8	$-0.20029777E-01$	$-0.15334104E-01$	$0.63130580E+00$	$-0.10368780E+00$
9	$-0.19079453E+00$	$-0.35359990E+00$	$0.73363091E+00$	$0.24531642E-02$
10	$0.82713210E-02$	$0.37227954E-01$	$0.68254260E-02$	$-0.17576068E-01$
11	$-0.30012859E-01$	$-0.83167416E-01$	$-0.29492493E+00$	
12	$0.19238860E-01$	$-0.23277092E-01$	$0.32181335E-02$	
13			$-0.25300562E-01$	
14			$-0.20206682E-01$	
481	$T_\mathrm{r} = T_\mathrm{c} = 1.0925$	$T_\mathrm{r} = T_\mathrm{c} = 1.0860$	$T_\mathrm{r} = T_\mathrm{c} = 1.0927$	$T_\mathrm{r} = T_\mathrm{c} = 1.0858$
	$\rho_\mathrm{r} = \rho_\mathrm{c} = 0.3496$	$\rho_\mathrm{r} = \rho_\mathrm{c} = 0.2964$	$\rho_\mathrm{r} = \rho_\mathrm{c} = 0.3048$	$\rho_\mathrm{r} = \rho_\mathrm{c} = 0.3078$
1	$0.10255408E+01$	$0.85770007E+00$	$0.89859893E+00$	$0.62879477E+00$
2	$-0.29883393E+01$	$-0.34235103E+01$	$-0.32980220E+01$	$-0.16369988E+01$
3	$0.93567437E+00$	$0.16935903E+01$	$0.13537245E+01$	$-0.48132993E-01$
4	$-0.40307217E-01$	$0.54495303E-01$	$0.51497465E-01$	$0.68799944E-01$
5	$0.10401008E+00$	$0.17731470E-03$	$0.53622643E-01$	$0.66281256E-04$
6	$0.60270067E-03$	$-0.81911732E-01$	$0.21657187E-03$	$0.23776802E+00$
7	$0.24151136E+00$	$0.14110767E+00$	$-0.34864858E-01$	$0.96122569E-01$
8	$-0.52932468E-01$	$-0.32082965E-01$	$0.20885830E+00$	$-0.96494864E-01$
9	$-0.20304201E+00$	$-0.11025131E+00$	$0.26059367E+00$	$0.63081633E-02$
10	$-0.45448678E-01$	$0.50742097E-02$	$-0.28835068E-01$	$-0.19306343E-01$
11	$-0.35478321E-01$	$-0.54316035E-01$	$-0.17205388E+00$	
12	$0.33959630E-01$	$-0.32609596E-01$	$-0.18945299E-01$	
13			$-0.58381045E-01$	
14			$-0.17638216E-01$	

Table 3: Parameters n_i of the SW_{12}, $\mathrm{SW}^{\mathrm{p}}_{12}$, SE_{14}, and S_{10} FEOS correlations eq. (3) obtained from weighted fits of α_{01} and α_{10} of eqs. (8). The numbering i is for consecutive terms in Table 1. The data set used has $D = 271$ (top) and $D = 481$ (bottom) state points as described in Figure 1 and Table 2. The fits are not constrained to a predetermined critical point. The reducing parameters $(T_\mathrm{r}, \rho_\mathrm{r})$ are identical with the critical points $(T_\mathrm{c}, \rho_\mathrm{c})$ of the correlations. Therefore, in reduced units, the critical point occurs at $\tau_\mathrm{c} = \delta_\mathrm{c} = 1$ in all cases.

	p			e^r			$(\partial e^\mathrm{r}/\partial v)_T$			c^r_v		
D	$\sigma_{1,271}$	$\sigma_{1,481}$	$\sigma_{1,705}$	$\sigma_{1,271}$	$\sigma_{1,481}$	$\sigma_{1,705}$	$\sigma_{1,271}$	$\sigma_{1,481}$	$\sigma_{1,705}$	$\sigma_{1,271}$	$\sigma_{1,481}$	$\sigma_{1,705}$
271	3.2	18.6	87.9	43.0	105.3	318.5	2.3	3.7	6.8	9.3	25.6	40.5
	5.5	38.3	150.8	36.9	123.2	397.5	2.7	5.6	9.0	13.0	34.7	56.1
	3.2	46.9	183.7	56.1	213.1	657.2	1.8	6.7	12.1	15.7	51.4	71.8
	3.4	19.1	75.1	27.9	48.2	85.4	1.6	2.2	4.0	7.1	7.6	21.6
481	5.8	10.2	73.2	62.8	73.2	212.4	4.5	3.9	6.1	9.7	19.9	38.2
	9.3	21.4	74.5	49.1	63.9	286.9	2.6	3.0	5.8	9.2	33.1	57.7
	7.7	11.9	61.0	67.5	80.8	323.3	2.7	3.0	6.3	9.9	34.6	63.6
	6.0	14.3	59.8	73.8	79.6	103.3	1.8	2.2	4.0	8.7	9.3	21.1
T_{21}	2.9	3.0	3.4	6.5	6.1	6.8	1.3	1.2	1.4	2.0	2.0	1.9

Table 4: FEOS correlation results from $D = 271$ and $D = 481$ state points as quantified in Table 2. Consecutive rows are for the FEOS correlations SW_{12}, $\mathrm{SW}^{\mathrm{p}}_{12}$, SE_{14}, and S_{10}. Only α^r_{01} (from pressure p) and α^r_{10} (from residual internal energy e^r) are used in those fits (542 and 962 independent thermodynamic properties). Fit assessments $\sigma_{1,M}$ are from eq. (9) and refer to the one indicated property compared at M state points. The last row (T_{21}) refers to our fully optimized benchmark correlation [15] with 21 terms fitted to $\alpha^\mathrm{r}_{01}, \alpha^\mathrm{r}_{10}, \alpha^\mathrm{r}_{11}, \alpha^\mathrm{r}_{20}$ at $D = 705$ state points (2820 independent thermodynamic properties).

T	p_s	ρ_v	ρ_l	ϕ_s	h_v	h_l	Δh_s
1.010	0.0646(1)	0.1055(3)	0.5594(5)	0.3325(3)	−1.254(4)	−4.253(2)	2.999(7)
1.015	0.0668(1)	0.1105(4)	0.5545(5)	0.3325(3)	−1.302(4)	−4.222(2)	2.920(7)
1.020	0.0689(1)	0.1162(4)	0.5467(7)	0.3314(4)	−1.362(5)	−4.180(3)	2.818(8)
1.030	0.0725(1)	0.1240(4)	0.5305(8)	0.3272(4)	−1.429(4)	−4.090(3)	2.661(8)
1.040	0.0771(1)	0.1379(7)	0.514(1)	0.3261(7)	−1.564(7)	−3.999(4)	2.44(1)
1.050	0.0819(1)	0.1543(7)	0.497(2)	0.325(1)	−1.716(7)	−3.898(5)	2.18(1)
1.060	0.0861(1)	0.1683(9)	0.468(2)	0.318(1)	−1.83(1)	−3.75(1)	1.92(2)
1.065	0.0893(1)	0.188(1)	0.461(2)	0.325(1)	−2.01(1)	−3.709(9)	1.71(2)
1.068	0.0904(1)	0.195(2)	0.438(2)	0.317(1)	−2.06(2)	−3.60(1)	1.54(3)
1.070	0.0918(1)	0.206(2)	0.438(2)	0.322(1)	−2.15(2)	−3.59(1)	1.44(3)
1.072	0.0927(1)	0.210(2)	0.428(5)	0.319(3)	−2.18(2)	−3.54(2)	1.36(4)
1.074	0.0934(2)	0.231(6)	0.404(3)	0.317(4)	−2.31(5)	−3.42(3)	1.11(8)
1.076	0.0944(2)	0.256(7)	0.411(4)	0.334(4)	−2.48(5)	−3.45(3)	0.97(8)

Table 5: New vapor-liquid equilibrium data for the LJTS model fluid. The molecular simulations were performed as before with our tool *ms2* [36, 38] using much larger simulation lengths and much larger system sizes. The subscript s stands for saturation. Whereas our previous VLE data extended from $T = 0.64$ to 1.06 [38], the present data cover the extended critical region from $T = 1.010$ to 1.076. Also shown is the computed rectilinear diameter $\phi_\mathrm{s} \equiv (\rho_\mathrm{v} + \rho_\mathrm{l})/2$ and enthalpy of evaporation $\Delta h_\mathrm{s} \equiv h_\mathrm{v} - h_\mathrm{l}$. Statistical simulation uncertainties are in the last digit: 0.97(8) means 0.97 ± 0.08. The highest temperature $T = 1.076$ corresponds to roughly $0.995T_\mathrm{c}$, where deviations of the FEOS correlations are largest. Using the same strategy as in reference [38], an updated critical point shifts insignificantly as $T_\mathrm{c} = 1.0779 \to 1.0800$, $\rho_\mathrm{c} = 0.3190 \to 0.3176$, $p_\mathrm{c} = 0.0935 \to 0.0969$, and $Z_\mathrm{c} = 0.272 \to 0.282$.

	T_m	p_m	ρ_m	T_s	p_s	ρ_s	T_JT
SW_{12}	2.405	1.145	0.386	0.881	0.0274	0.675	5.260
$\mathrm{SW}^\mathrm{P}_{12}$	2.426	1.129	0.381	0.876	0.0267	0.680	4.933
SE_{14}	2.362	1.142	0.392	0.876	0.0265	0.680	5.117
S_{10}	2.500	1.148	0.374	0.880	0.0272	0.678	5.346
T_{21}	2.413	1.166	0.389	0.882	0.0276	0.678	5.254

Table 6: Specific points on the Joule-Thomson inversion curves, as calculated from the FEOS correlations from $D = 481$ state points in Table 3 and displayed in Figure 10: Maximum (m), intersection with the bubble line (s), duplication of the Joule-Thomson inversion temperature at zero density from the exact eqs. (15) ($T_\mathrm{JT} = 5.256$) and Table 2. The last row (T_{21}) refers to our fully optimized benchmark correlation with 21 terms [15].

	SW_{12}	SW^{p}_{12}	SE_{14}	S_{10}	T_{21}
	(1) α^{r}_{01}, α^{r}_{10}				
$\sigma_{2,481}$	52	47	57	57	
$\sigma_{4,481}$	38	37	44	40	
$\sigma_{2,705}$	158	209	232	84	
$\sigma_{4,705}$	113	150	167	60	
T_c	1.093	1.086	1.093	1.086	
ρ_c	0.350	0.296	0.305	0.308	
p_c	0.104	0.099	0.102	0.101	
Z_c	0.273	0.308	0.307	0.301	
T_B	2.82	2.68	2.78	2.84	
T_{JT}	5.26	4.93	5.12	5.35	
	(2) α^{r}_{01}, α^{r}_{10}, α^{r}_{11}				
$\sigma_{2,481}$	54	48	56	57	
$\sigma_{4,481}$	39	37	43	41	
$\sigma_{2,705}$	160	208	229	84	
$\sigma_{4,705}$	115	149	165	60	
T_c	1.093	1.086	1.092	1.086	
ρ_c	0.349	0.297	0.306	0.308	
p_c	0.105	0.099	0.102	0.101	
Z_c	0.272	0.308	0.305	0.301	
T_B	2.82	2.68	2.78	2.84	
T_{JT}	5.26	4.93	5.11	5.34	
	(3) α^{r}_{01}, α^{r}_{10}, α^{r}_{20}				
$\sigma_{2,481}$	40	53	60	28	
$\sigma_{4,481}$	29	39	44	20	
$\sigma_{2,705}$	135	165	180	76	
$\sigma_{4,705}$	97	119	130	55	
T_c	1.106	1.075	1.083	1.086	
ρ_c	0.342	0.250	0.264	0.310	
p_c	0.112	0.093	0.096	0.101	
Z_c	0.295	0.344	0.337	0.300	
T_B	2.81	2.63	2.71	2.82	
T_{JT}	5.25	4.88	5.03	5.32	
	(4) α^{r}_{01}, α^{r}_{10}, α^{r}_{11}, α^{r}_{20}				
$\sigma_{2,481}$	39	53	62	28	4.8
$\sigma_{4,481}$	28	39	46	20	3.5
$\sigma_{2,705}$	135	165	180	76	5.4
$\sigma_{4,705}$	97	119	130	54	4.0
T_c	1.105	1.077	1.083	1.086	1.086
ρ_c	0.342	0.254	0.264	0.310	0.319
p_c	0.112	0.094	0.096	0.101	0.101
Z_c	0.295	0.342	0.336	0.300	0.292
T_B	2.81	2.63	2.71	2.82	2.78
T_{JT}	5.25	4.88	5.03	5.32	5.25

Table 7: Several scenarios (1) to (4) further assess the correlations considered in this work. The underlying data set consists of $D = 481$ state points as quantified in Table 2. All simulated properties α^{r}_{01} (from pressure p), α^{r}_{10} (from residual internal energy e^{r}), α^{r}_{11} (from volume derivative of residual internal energy $(\partial e^{r}/\partial v)_T$), and α^{r}_{20} (from residual isochoric heat capacity $c^{r}_{v} \equiv (\partial e^{r}/\partial T)_v$) are used in various combinations. Note that scenarios (2) and (3) have never been tried before with molecular simulation data. Scenario (4) was first used for our fully optimized benchmark correlation T_{21} [15]. Fit assessments $\sigma_{2,481}$ and $\sigma_{2,705}$ are as in Table 2, using p, e^{r}, whereas $\sigma_{4,481}$ and $\sigma_{4,705}$ are obvious extensions of eq. (9) to $(\partial e^{r}/\partial v)_T$, and c^{r}_{v}, including all molecular simulation results in all fits. Among the generalized correlations for the LJTS model fluid S_{10} performs best.

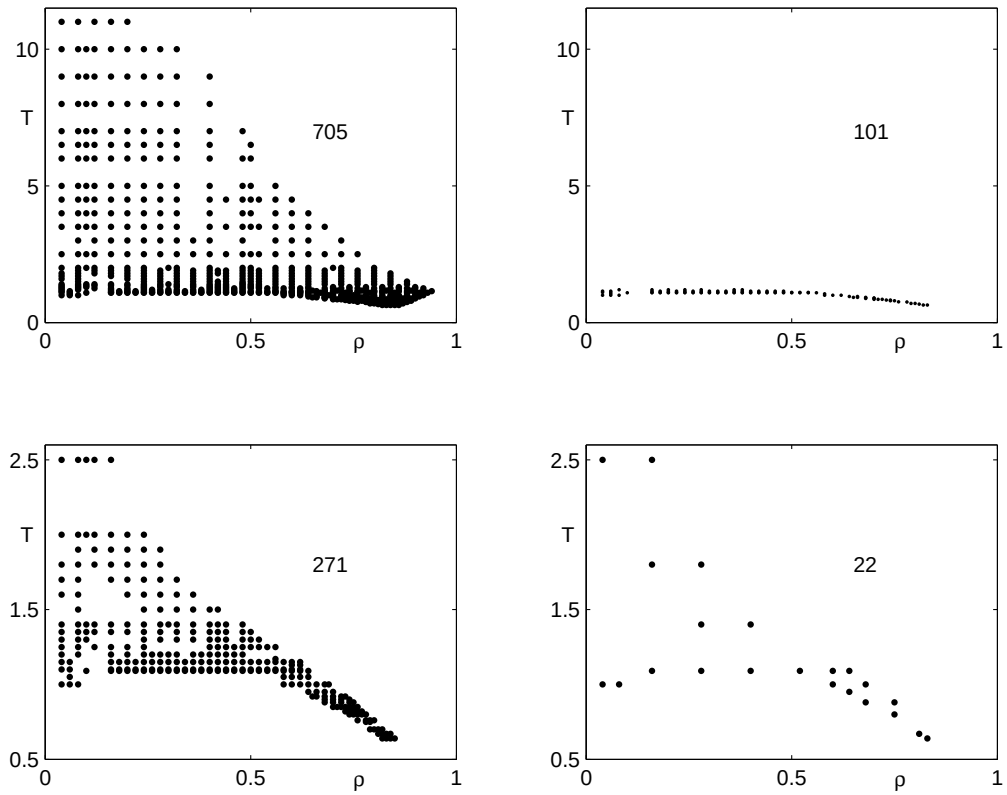

Figure 1: T, ρ state points used for FEOS correlation in this work. Four independent thermodynamic properties at each state point are available: Pressure p, residual internal energy e^{r}, isothermal volume derivative of the latter $(\partial e^{\mathrm{r}}/\partial v)_T$, and isochoric heat capacity $c_v^{\mathrm{r}} = (\partial e^{\mathrm{r}}/\partial T)_v$. The original data set is 705 state points. Maximum temperature $T = 11$ corresponds to about 2000 Kelvin and maximum pressure $p = 6.8$ (northeast border of states is isobaric) corresponds to about 3000 bar if methane is used as a representative for the LJTS model fluid. Such states are beyond any practical application. A dramatic shrinkage of state points from 705 to 101 (top) and thinning from 271 to 22 (bottom) is shown. Consequences for FEOS correlation are discussed around Table 2.

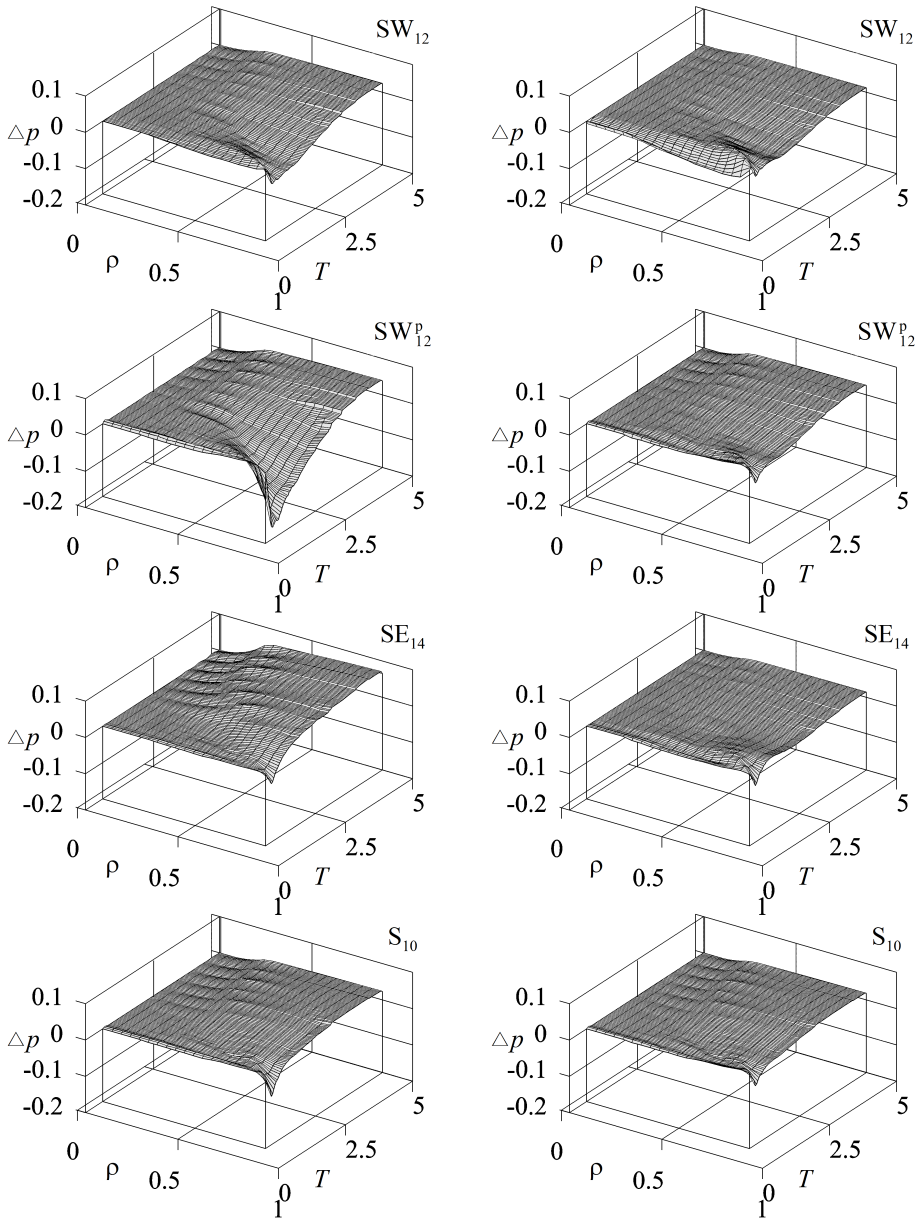

Figure 2: Pressure deviations $\Delta p(T,\rho) \equiv p(T,\rho) - p^{\mathrm{FEOS}}(T,\rho)$ between molecular simulation raw data and correlation (FEOS) results. The parameters of the FEOS correlations are from p and e^{r} at $D = 271$ state points (left) and $D = 481$ state points (right) as quantified in Table 2. Note that molecular simulation uncertainties Δ_p as defined in section 5 are too small to be visible on the scale of the plot. None of the displayed state points is within the vapor-liquid two-phase region of any of the correlations.

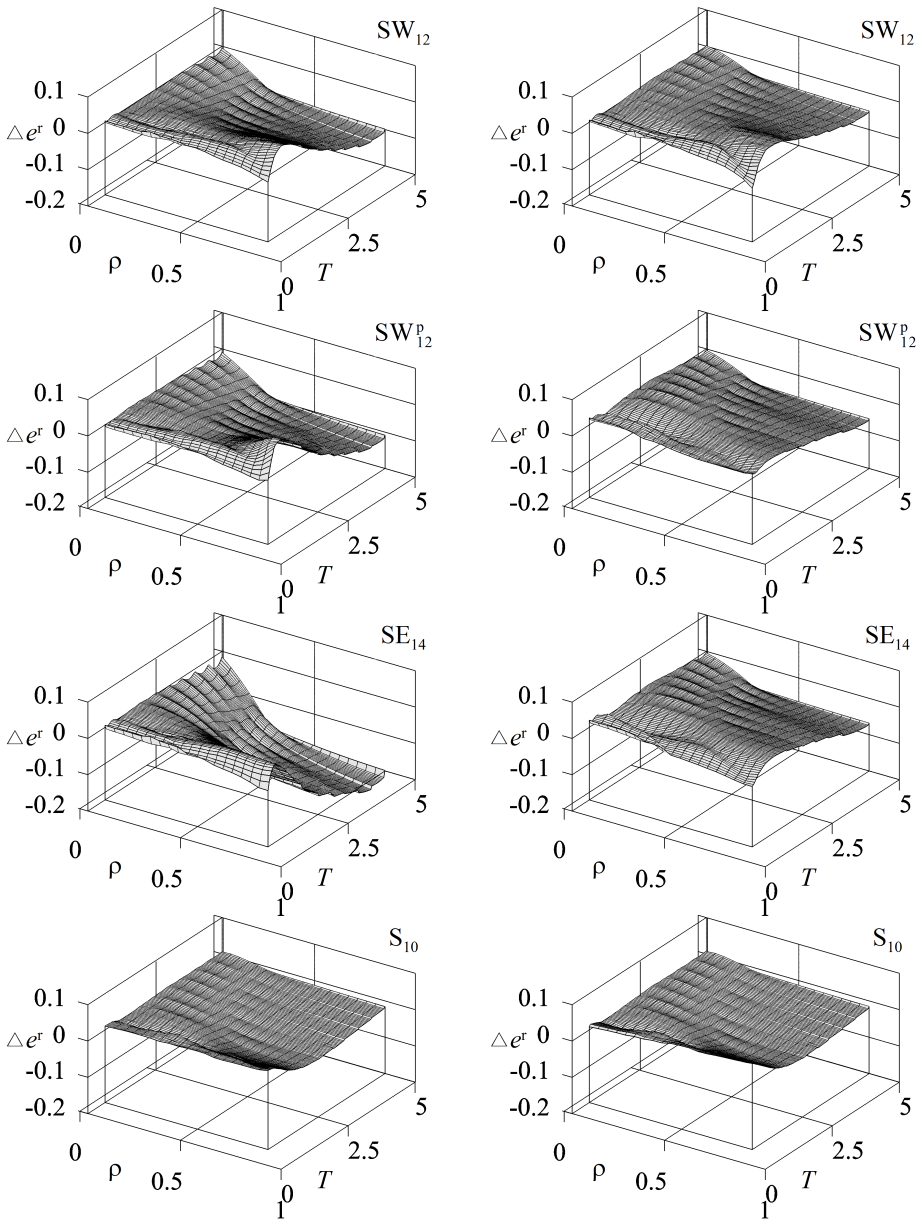

Figure 3: Residual internal energy deviations $\Delta e^{\mathrm{r}}(T,\rho) \equiv e^{\mathrm{r}}(T,\rho) - e^{\mathrm{r,FEOS}}(T,\rho)$. Details are as in Figure 2.

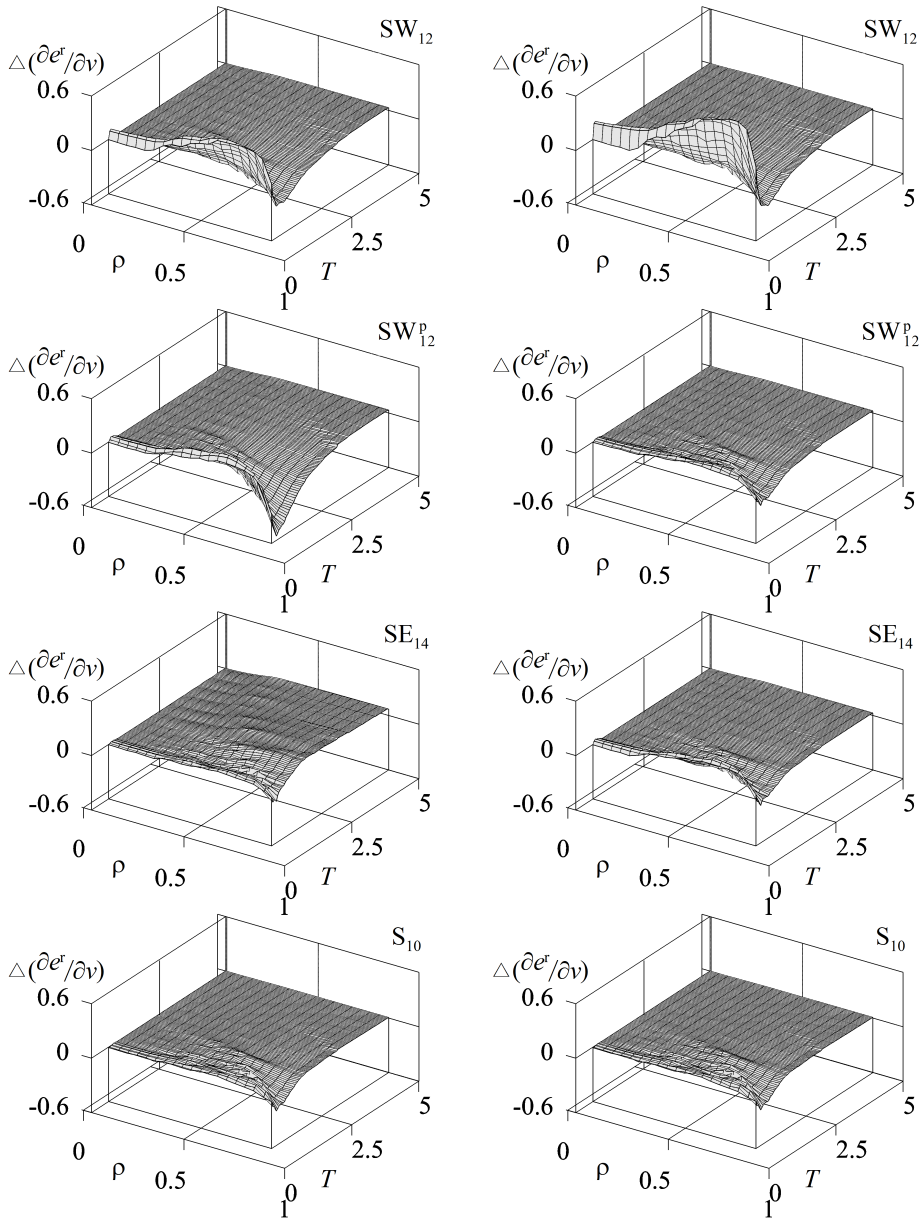

Figure 4: Deviations in volume derivative of the residual internal energy $\Delta(\partial e^{\mathrm{r}}/\partial v)_T(T,\rho) \equiv (\partial e^{\mathrm{r}}/\partial v)_T(T,\rho) - (\partial e^{\mathrm{r,FEOS}}/\partial v)_T(T,\rho)$. Details are as in Figure 2.

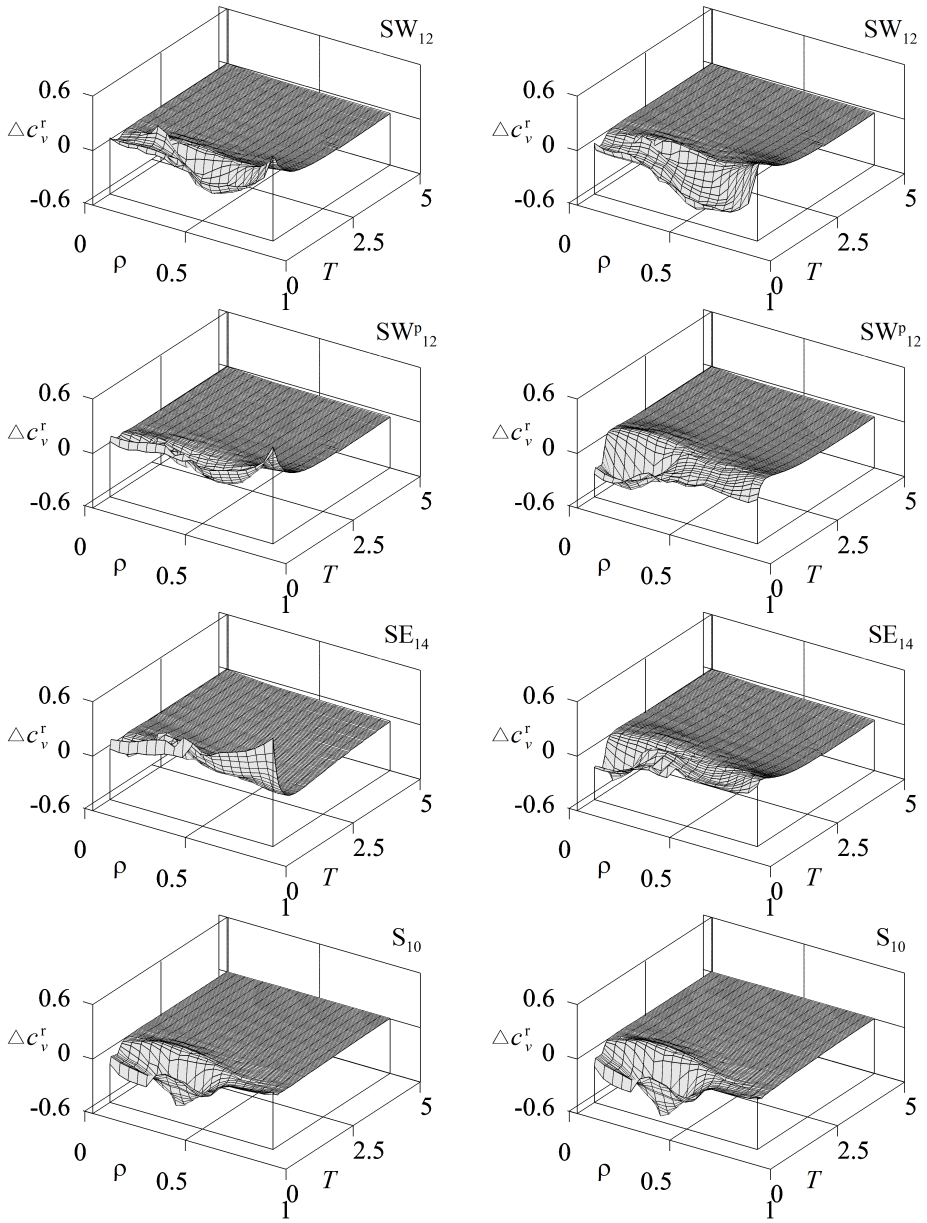

Figure 5: Deviations in residual isochoric heat capacity $\Delta c_v^{\mathrm{r}}(T,\rho) \equiv c_v^{\mathrm{r}}(T,\rho) - c_v^{\mathrm{r,FEOS}}(T,\rho)$. Details are as in Figure 2.

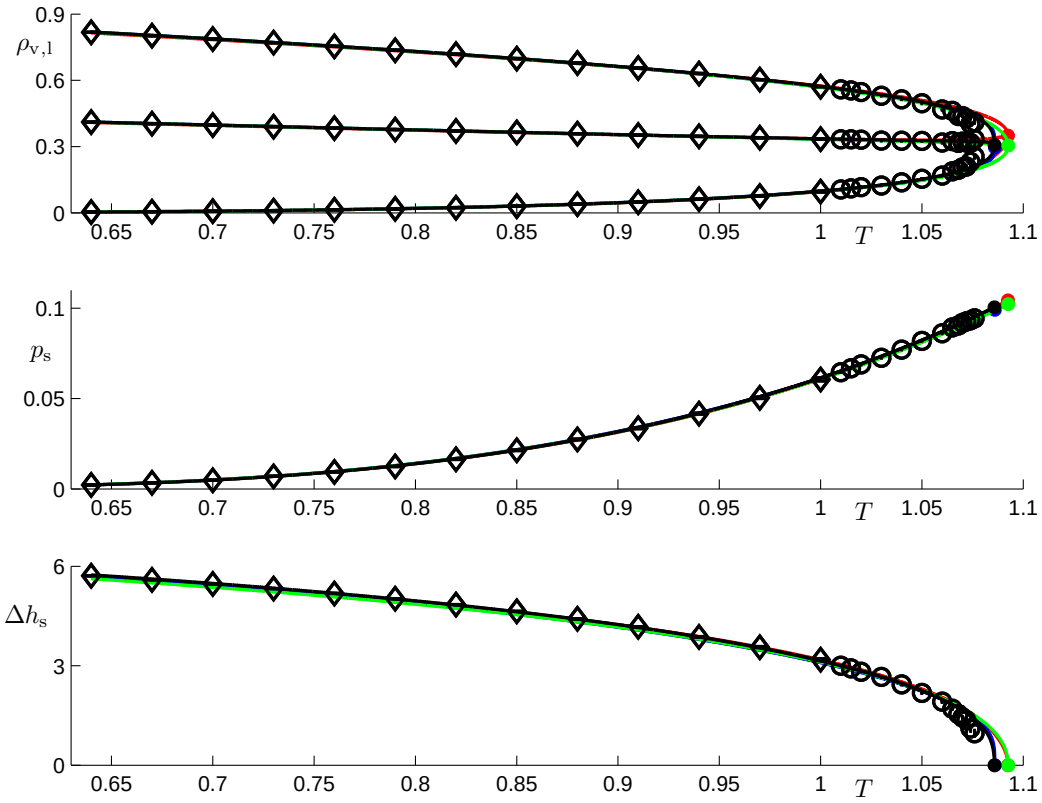

Figure 6: Vapor-liquid equilibrium for the LJTS system: Saturated density $\rho_{v,l}$ and rectilinear diameter $\phi \equiv (\rho_v + \rho_l)/2$ (top), vapor pressure p_s (middle), evaporation enthalpy Δh_s (bottom). Symbols are molecular simulation results from reference [38] (diamonds) and Table 5 (circles). Lines are the FEOS correlations.

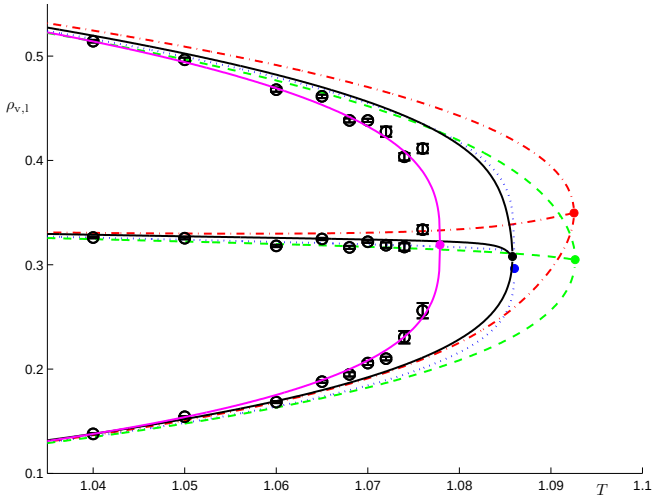

Figure 7: Vapor-liquid equilibrium for the LJTS system in the extended critical region: Symbols are saturated densities $\rho_{v,l}$ and rectilinear diameters $\phi \equiv (\rho_v + \rho_l)/2$ from Table 5. Lines represent correlations. SW_{12}: dash-dotted, SW_{12}^{p}: dotted, SE_{14}: dashed, S_{10}: solid. The solid line passing closest through the symbols represents the independent density correlations of Vrabec *et al.* [38]. Full bullets represent the critical points from the correlations.

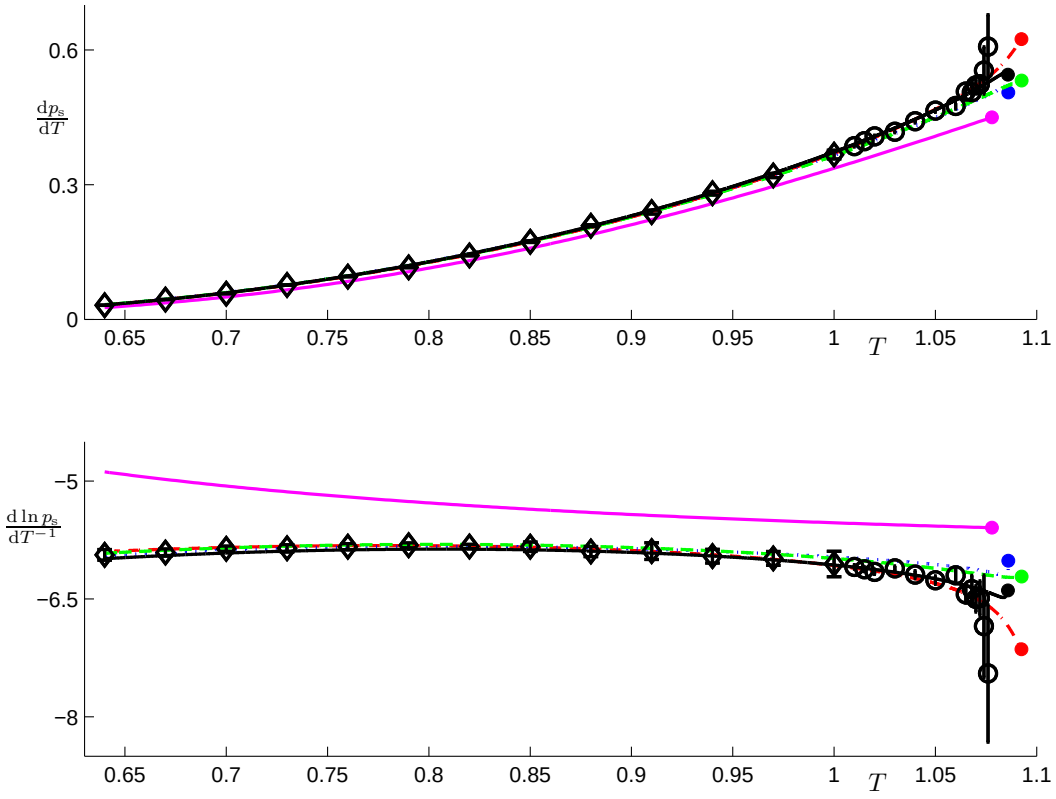

Figure 8: Consistency test using the Clapeyron eq. (11). Symbols are direct molecular simulation results of Vrabec *et al.* [38]. Lines represent correlations. SW_{12}: dash-dotted, SW^{P}_{12}: dotted, SE_{14}: dashed, S_{10}: solid. The solid line not passing through the symbols represents an independent vapor pressure correlation [38]. Full bullets represent critical points as determined from the FEOS correlations.

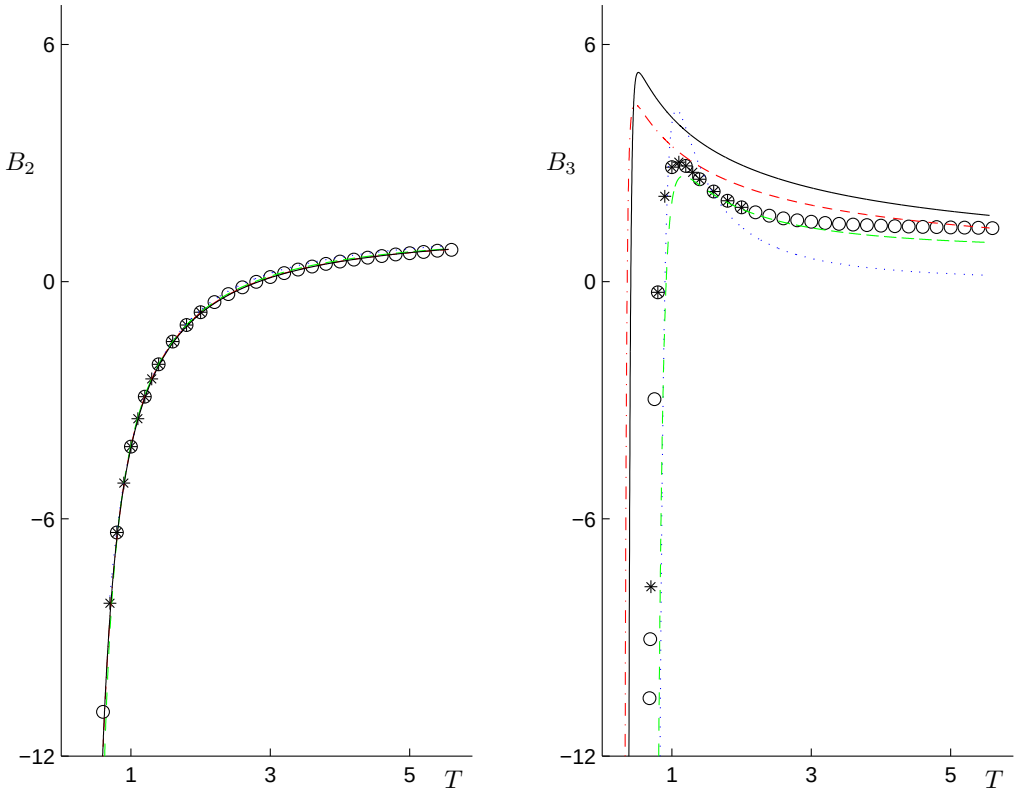

Figure 9: Second and third virial coefficients from rigorous computation and FEOS correlations. Symbols are exact results. Stars: reference [58], open circles: numerical solution of eqs. (14). Lines represent correlations. SW_{12}: dash-dotted, SW_{12}^{p}: dotted, SE_{14}: dashed, S_{10}: solid.

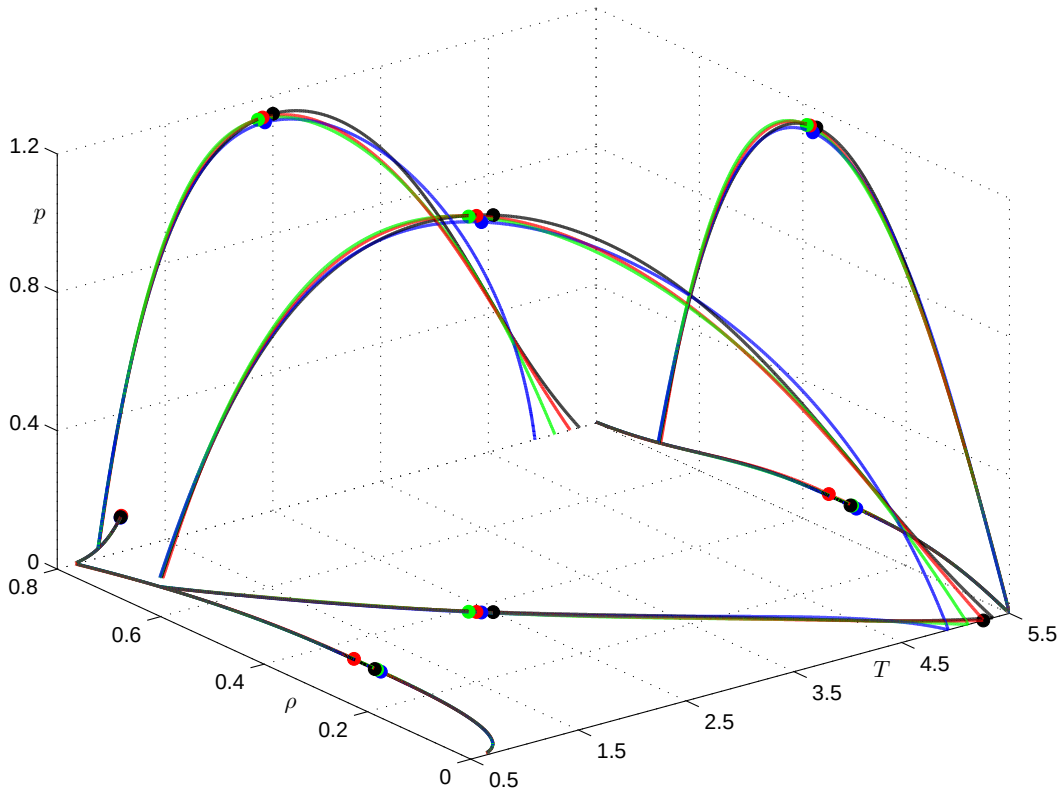

Figure 10: Three-dimensional Joule-Thomson inversion curves, $\mu_{\rm JT} \equiv (\partial T/\partial p)_h = 0$, and their projections as computed from the FEOS correlations. $\rm SW_{12}$: red, $\rm SW_{12}^{P}$: blue, $\rm SE_{14}$: green, $\rm S_{10}$: black. Also included are the projections of VLE data in Figures 6 and 7 for orientation. Bullets denote maxima and critical points. The single bullet on the temperature axis is the exact Joule-Thomson inversion temperature at zero density, $T_{\rm JT} = 5.256$, as computed from eqs. (15). The facts that the $\rm SW_{12}$ FEOS hits that point precisely and all FEOS correlations appear to intersect in one point are satisfying but accidental. Numerical details are in Table 6.